



HAL
open science

Steady state operation of a copper-water LHP with a flat-oval evaporator

Suzanne Becker, S. Vershinin, V. Sartre, E. Laurien, Jocelyn Bonjour, Yu.F. Maydanik

► **To cite this version:**

Suzanne Becker, S. Vershinin, V. Sartre, E. Laurien, Jocelyn Bonjour, et al.. Steady state operation of a copper-water LHP with a flat-oval evaporator. *Applied Thermal Engineering*, 2011, 31 (5), pp.686-695. 10.1016/j.applthermaleng.2010.02.005 . hal-00541908

HAL Id: hal-00541908

<https://hal.science/hal-00541908>

Submitted on 3 Oct 2013

HAL is a multi-disciplinary open access archive for the deposit and dissemination of scientific research documents, whether they are published or not. The documents may come from teaching and research institutions in France or abroad, or from public or private research centers.

L'archive ouverte pluridisciplinaire **HAL**, est destinée au dépôt et à la diffusion de documents scientifiques de niveau recherche, publiés ou non, émanant des établissements d'enseignement et de recherche français ou étrangers, des laboratoires publics ou privés.

Manuscript Number: ATE-2009-589R2

Title: Steady state operation of a copper-water LHP with a flat-oval evaporator

Article Type: Research Paper

Keywords: loop heat pipe; avionic application; Heat transfer; experimental study; tilt angle effect; heat sink temperature effect

Corresponding Author: Ms. Susanne Becker, M.Sc.

Corresponding Author's Institution: IKE

First Author: Susanne Becker, M.Sc.

Order of Authors: Susanne Becker, M.Sc.; Sergei Vershinin; Valérie Sartre, Associate Professor; Eckart Laurien, Professor; Jocelyn Bonjour, Professor; Yuri F Maydanik, Professor

Abstract: In order to dissipate the heat generated by electronic boxes in avionic systems, a copper-water LHP with a flat-oval evaporator was fabricated and tested at steady-state. The LHP consists of a flat shaped evaporator, 7 mm thick, including compensation chamber with attached heat exchanger. The condenser is cooled by forced convection of liquid. The variable parameters are the heat sink and ambient temperatures (20 and 55 °C), the orientation (-90° to +90° in two perpendicular planes) and the power input (0 to 100 W). Evaporator wall temperatures are higher when the evaporator is placed above the condenser. For heat sink and ambient temperature of 20 °C the evaporator wall temperature does not vary much with heat load for all measured elevations. But it fluctuates at heat sink and ambient temperature equal to 55 °C when the evaporator is placed below the condenser. The LHP total thermal resistance is governed by the condenser resistance. It decreases with increasing heat load, whatever the operating conditions, because the part of the condenser internal surface area used for condensation increases too. A minimum thermal resistance of 0.2 K/W was obtained. The maximum thermal resistance was 2.7 K/W.

Steady state operation of a copper-water LHP with a flat-oval evaporator

S. Becker^{a,*}, S. Vershinin^b, V. Sartre^c, E. Laurien^a, J. Bonjour^c, Yu.F. Maydanik^b

^a *Institute of Nuclear Technology and Energy Systems (IKE), Department of Energy Conversion and Heat Transfer, University of Stuttgart, Pfaffenwaldring 31, 70569 Stuttgart, Germany*

^b *Institut of Thermal Physics (ITP), Ural Branch, Russian Academy of Sciences, Amundsen St. 106, Ekaterinburg, 620016, Russia*

^c *Université de Lyon, CNRS, INSA-Lyon, CETHIL, UMR5008, F-69621, Villeurbanne, France*

Abstract

In order to dissipate the heat generated by electronic boxes in avionic systems, a copper-water LHP with a flat-oval evaporator was fabricated and tested at steady-state. The LHP consists of a flat shaped evaporator, 7 mm thick, including compensation chamber with attached heat exchanger. The condenser is cooled by forced convection of liquid. The variable parameters are the heat sink and ambient temperatures (20 and 55 °C), the orientation (-90° to +90° in two perpendicular planes) and the power input (0 to 100 W). Evaporator wall temperatures are higher when the evaporator is placed above the condenser. For heat sink and ambient temperature of 20 °C the evaporator wall temperature does not vary much with heat load for all measured elevations. But it fluctuates at heat sink and ambient temperature equal to 55 °C when the evaporator is placed below the condenser. The LHP total thermal resistance is governed by the condenser resistance. It decreases with increasing heat load, whatever the operating conditions, because the part of the condenser internal surface area used for condensation increases too. A minimum thermal resistance of 0.2 K/W was obtained. The maximum thermal resistance was 2.7 K/W.

* Corresponding author; Tel.: (+49) 711 685-62127; Fax: (+49) 711 685-62010
E-mail address: susanne.becker@ike.uni-stuttgart.de

Keywords: loop heat pipe, avionic application, heat transfer, experimental study, tilt angle effect, heat sink temperature effect

Nomenclature

c_p	specific heat capacity	J/(kg K)	Subscripts	
I	electrical current	A	<i>amb</i>	ambient air
p	pressure	Pa	<i>cool</i>	coolant
P_{el}	electrical power	W	<i>evap</i>	evaporator
\dot{Q}	thermal heat flow	W	<i>in</i>	input or inlet
R_{th}	thermal resistance	K/W	<i>out</i>	output or outlet
T	temperature	°C	<i>tot</i>	<i>total</i>
U	electrical voltage	V	<i>V</i>	vapour
\dot{V}	volumetric flow rate	m ³ /s	<i>W</i>	wall
Greek			Abbreviations	
γ	orientation in y-z direction	degree	<i>CC</i>	compensation chamber
δ	orientation in x-z direction	degree	<i>CCHS</i>	heat sink of the compensation chamber
ρ	density	kg/m ³	<i>CW</i>	cooling water
			<i>Evap</i>	evaporator
			<i>HS</i>	heat sink
			<i>LL</i>	liquid line
			<i>VL</i>	vapour line

1. Introduction

New generations of In-flight Entertainment Systems (IFE) are required to provide more and more services (audio, video, Internet, flight services, multimedia, games, shopping, phone ...) at an affordable cost. But unlike other avionics systems installed in controlled-temperature bays, most of the IFE equipment and boxes are not connected to the aircraft cooling system. This situation creates thermal management problems that affect the reliability and the safety of the equipment. The most critical equipment is the Seat Electronic Box (SEB) installed under each passenger seat as shown in Figure 1. The heat flux dissipated by these boxes can reach 30 W and might reach up to 100 W (6.25 W/cm^2) in the close future.

An alternate advanced cooling technique to the fans is based on loop heat pipes (LHP) systems. LHP can adequately be integrated inside the seat structure and may take benefit of the seat frame as a heat sink. The LHP is a passive two-phase heat transfer device that utilizes the evaporation and condensation of a working fluid to transfer heat, and the capillary forces developed in a porous wick to circulate the fluid. The LHP is known for its high pumping capability and robust operation because it uses fine-pored wicks and the integrated evaporator/reservoir design.

Amongst all the existing LHP designs, the LHP having flat evaporator surfaces are more adapted to electronic cooling applications [1], [2]. Flat plate evaporators provide both a shorter and a more uniform thermal path from a flat component to the vaporization interface in the evaporator. The flat disk-shaped evaporator was already invented in the USSR in 1975, when the term of "loop heat pipe" was not used yet. At that time, such evaporators did not arouse much interest in the scientific community. Twenty years later, a water LHP with a disk-shaped evaporator, 48 mm in diameter, designed to cool a powerful thyristor, was the subject of a Russian patent. This flat disk-shaped evaporator had already the quite modern design used

nowadays. On the basis of technical solutions presented in another patent [3] that describes variants of the flat disk-shaped evaporator, Maydanik et al. fabricated and tested about 10 LHP's, 30 mm in diameter and 10 to 13 mm thick, using ammonia as working fluid [4, [5]. Delil et al. [6] obtained the best performance for capillary structures with small pore sizes, which had in addition a better ability to operate against gravity than capillary structures with large pore sizes. Their device was able to transfer about 8 W/cm² and its thermal resistance laid in the range 0.62 – 1.32 K/W. To cool computer CPUs, Pastukhov et al. [7, 8] investigated 7 mm thick LHPs with different evaporator cross sections (flat rectangular or flat oval) and materials (stainless steel or copper). Tsai et al. [9] fabricated a low cost miniature flat plate LHP, whose wick was made of a copper mesh screen. A wick of similar design was fabricated by Young et al. [10], in which two stainless steel porous plates were welded to a U-shaped porous sidewall. The evaporator, 6 mm thick, could be heated on both sides for applications like cooling of fuel cells stacks. A LHP minimum thermal resistance of 1.27 K/W was obtained for a heat flux of 1.56 W/cm². It was found that this resistance may be affected by the fluid fill charge. Boo and Chung [11] tested a LHP with a flat evaporator, 30 mm thick, and a propylene wick, filled with various working fluids (methanol, ethanol, acetone, water). A maximum heat flux of 6.5 W/cm² was achieved using methanol. The thermal resistance was of 0.9 K/W and did not change much with the fluid fill charge, as the reservoir was located above the wick. Singh et al. [12], [13] developed a copper/water LHP with a disk shaped evaporator, 10 mm thick and a nickel porous wick. The device was tested under uniform and non-uniform heating modes [12]. Using forced air convection, a minimum total thermal resistance of 1.2 K/W, corresponding to a heat pipe thermal resistance of 0.17 K/W, was achieved at about 10 W/cm². An evaporating thermal resistance of 0.06 K/W was deduced from the experimental measurements. In the attempt to reduce the evaporator thickness to 5 mm, due to space constraints in laptop computers, Singh et al. [14] fabricated a copper/water LHP where the nickel porous wick occupied the whole evaporator thickness (2.5 mm). The compensation chamber provided liquid

access to the wick from three side faces. The total thermal resistance at 10 W/cm^2 was 1.5 K/W , corresponding to a heat pipe thermal resistance of 0.62 K/W .

The LHP evaporators described previously had an inverted meniscus arrangement, in which liquid and vapour flows are in the opposite direction of the heat flow. In non-inverted meniscus evaporators, patented in the US by Phillips [15] in 2003 and in Russia by Maydanik [16], the heat flow enters from the liquid side of the meniscus, like classical heat pipes. This evaporator concept was already tested in Russia in the late seventies, early eighteens of the last century [17, 18]. As compared to the inverted meniscus arrangement, the non-inverted meniscus arrangement leads to decrease of the evaporator thermal resistance and allows shifting the dry-out limitation due to wick deprime. Vasiliev reported a maximum heat flow rate of 35 W/cm^2 [19]. Tang et al. [20] developed a capillary two phase loop consisting of a cylindrical copper evaporator with water as the working fluid. A primary wick layer with fine pores covered the inner face of the heated zone and provided a barrier facing the vapour volume. A secondary wick of higher permeability was used to feed the primary wick. This device was able to dissipate a heat flux of 16 W/cm^2 . In the copper evaporator developed by Doktorau et al. [21], a thick copper wick layer was disposed to separate the compensation chamber and the vapour space, while a thin wick layer would distribute the liquid over the whole heated surface. A heat dissipation of 140 W with a heat transfer area of about 1 cm^2 was achieved. The evaporator thermal resistance had a very low value of 0.05 K/W . The Phillips flat plate evaporator concept [15] differs from that of Doktorau et al. [21] by the design of the secondary wick, which plays a double role. It separates the liquid from the vapour volumes, and feeds liquid to the primary wick at several locations along the heated zone. In the evaporator proposed by Li [22], the capillary structure, of cylindrical shape, is contained in a retaining hole drilled into the evaporator body. For these LHP evaporators, no experimental results are available in the literature until now.

For the present work, a copper/water LHP with a flat-oval evaporator was fabricated at the Institute of Thermal Physics (ITP) and tested at the Institute of Nuclear Technology and Energy Systems (IKE). Details of the evaporator are shown in Figure 2. As compared to the previous studies, the evaporator design combines the flat heat transfer area and the non-inverted meniscus principle. The evaporator is called flat – oval as the heat is supplied directly to the flat case of the evaporator without any saddle that is necessary for cylindrical evaporators. The evaporator is referred to as “oval” because of the shape of its cross section. Furthermore the LHP includes additional new features. A hole is drilled along the tube inside the reservoir to ensure cold liquid supply to the wick, whatever the LHP orientation. The compensation chamber is equipped with a finned radiator in order to reduce the LHP operating temperature. The test bench and the experimental parameters were defined in order to provide data for the steady-state numerical model developed at the Centre de Thermique de Lyon (CETHIL). The present paper describes the experimental test bench which was developed and the test results of the LHP.

2. LHP experimental study

2.1 Description of the tested LHP

The tested LHP consists of a flat shaped evaporator including compensation chamber with attached heat exchanger. The tubing, which designates the vapour line, the line of the condenser section as well as the liquid line has a circular cross section. All components of the LHP including wick material are made of copper except the plate welded to the condenser section which is made of aluminium. Figure 3 shows the LHP from below, the top view and the condenser box.

The dimensions of the LHP are listed in Table 1. Water is used as a working fluid.

2.2 Description of the experimental set-up

General description of the test bench

The heat source is a copper block attached to the evaporator, heated with a cartridge. The heat sink of the LHP is cooled by a cryostat. The condenser cooling by a liquid circulation, although not representative of the real system which is free convection of air, was selected because the boundary conditions at the condenser can be better controlled in this way. Furthermore, the uncertainties on the heat balance are reduced. Temperatures are measured at different positions of the LHP using calibrated type K (Ni/CrNi) thermocouples. Altogether 18 thermocouples are directly attached to the LHP.

The whole construction is embedded into a box made of Plexiglas ($1 \times 1 \times 0.6 \text{ m}^3$), where different ambient conditions can be set. The box is isolated with a high efficient isolation material to avoid as much as possible heat transfer between the box and the ambient. Flanges are employed at the front side and at the top of the box, so that the experimental parameters inside the box can be set easily to the requested experimental conditions.

Several feedthroughs are employed to connect the lines for the measurement sensors and the heating and cooling devices.

Instrumentation and location of the thermocouples

Figure 4a shows the instrumentation of the test rig. The power supply unit is connected to the cartridge heater. It is controlled by the data logger. The thermostat controls the temperature of the coolant at the condenser section. Its volumetric flow rate is measured by a magnetic inductive flow meter. Two resistant temperature sensors (Pt100) measure the inlet and outlet coolant temperature. By the help of the cryostat, the ambient temperature inside the box is set. A resistant temperature sensor (Pt100) located near the LHP is connected to the cryostat, measuring the input temperature for the control loop of the cryostat. Furthermore there are three

calibrated thermocouples (Type K – Ni/CrNi) measuring the ambient temperature inside the box placed near the top, in the middle and at the bottom. All signals are measured by a data logger inclusive the room ambient temperature which is measured by a resistant temperature sensor (Pt100). Figure 4b depicts the external view of the test rig.

Additional calibrated thermocouples (Type K – Ni/CrNi) are connected to the LHP in order to measure the temperature distribution along it. Figure 5 shows the positions of the thermocouples. The upper sketch shows the top view; the sketch below shows the front view of the LHP.

Controlled parameters and their range of variation

Table 2 gives an overview of parameters which have been varied in the following, namely the type of cooling, the coolant and box ambient temperature, the orientation and the power input.

For a better thermal analysis both the vapour and the liquid lines were insulated. That allows the assumption of an adiabatic flow in the pipes. The inlet and the outlet temperature of the coolant as well as its volume flow were measured, allowing a calculation of the heat output at the condenser.

The variation of the coolant and ambient temperature is representative of RTCA DO160D[†] specification. That standard dictates among other things the operation range of electronics equipment in aircrafts between -15°C and 55 °C cabin temperature. One task of the FP6 European COSEE project was to test the LHP at ambient and heat sink temperatures of 20°C and 55°C.

In order to investigate the LHP for start and landing conditions, as well as for right and left benches during the flight, the LHP was tested under different angles in y - z as well as in x - z direction as shown in Figure 6. The angles range from -90° up to +90° in order to highlight the effect of gravity.

[†] RTCA: Radio Technical Commission for Aeronautics

As exposed in the introduction section, the maximum power input of 100 W is the maximum expected heat flow produced by the electronic components of SEB.

2.3 Experimental procedure

The LHP was adjusted to the orientation of interest and the box ambient temperature was set. As all temperatures of the LHP showed the same value as the box ambient temperature ($\Delta T_{max} = 1\text{K}$) the first power input step of 20 W was applied to the evaporator. Once all temperatures reached a stationary value (or oscillating stationary value) the power input was increased by a step of 20 W. The maximum power input was fixed to 100 W. Nevertheless, if the evaporator temperature reached 100 °C (which is the maximum operating temperature of the LHP), an emergency system was to turn off the experiment.

The electrical power P_{el} applied to the cartridge has been calculated by measuring the current and the voltage:

$$P_{el} = IU \tag{1}$$

Assuming no heat losses through the insulation at the heating zone, the applied electrical power is taken as the thermal heat applied to the LHP \dot{Q}_{in} .

Including the accuracy of the thermocouples and the uncertainties of the data logger, the uncertainty of the temperature is evaluated to 0.1 K. The uncertainty of the electrical power input is evaluated to 0.8×10^{-3} W including the uncertainty of the power supply unit and the uncertainty of the data logger.

4. Experimental results

4.1 Evaporator temperature

The temperatures indicated in the following are temperatures measured at steady state. This means that the derivative of all temperatures measured along the LHP with respect to time is zero. It must be mentioned that in some measurements, an oscillating temperature distribution with respect to time was observed. In such cases, steady state was defined when the height of the amplitudes and the wavelength stayed constant. As the system reached steady state, at least one thousand more measurement points were taken. From these measurement points, the last hundred points were taken for the mean calculation of the temperatures indicated here as the steady state temperature at a certain position.

The evaporator temperature indicated in the following figures is measured on top of the evaporator in the centre of the heated area. Because two cartridges are inserted inside the insulated copper block, this temperature is not necessarily the maximum temperature of the heated area, but it can be taken as the mean temperature along the evaporator heating area.

The syntax of the legend in the following figures can be explained as follows: the first two numbers describe the angle δ while the second two numbers specify the angle γ of the LHP as defined in Figure 6.

Figure 7 shows a small variation of the evaporator temperature (max. 5 K) at different heat inputs for angles $\gamma \geq 0^\circ$ (evaporator above condenser). The LHP is still in auto-regulation regime over the whole heat load range, which means the LHP operates at variable conductance mode. For negative angles ($\gamma < 0^\circ$), the temperature variation of the evaporator reaches a maximum range of 15 K. Furthermore the evaporator temperature increases with increasing heat load indicating the beginning of heat-pipe mode with a fully open condenser called fixed

conductance mode. The peak at an angle γ of -30° and at a heat load of 40 W, which is the same value as for $+30^\circ$ is an unexpected phenomenon and needs further investigation.

It can also be seen that the evaporator temperatures at positive angles are higher than those measured for negative angles. This effect results from gravitational assistance to the transport of working fluid inside the liquid line at negative angles. In addition the evaporator temperatures at an angle $\gamma = 60^\circ$ are higher than those of 90° which results from the lowest coolant flow applied to the condenser. It was $0.03 \text{ m}^3/\text{h}$ for 60° , $0.09 \text{ m}^3/\text{h}$ for 0° and 30° and $0.12 \text{ m}^3/\text{h}$ for the other angles (-90° , -60° , -30° , $+90^\circ$). The variation of coolant flow occurred due to technical reasons. Furthermore, the evaporator temperatures do not exceed 85°C which is typically the maximum allowed evaporator temperature for aircraft electronic equipment.

Figure 8 shows almost no influence of the variation of angle δ on the evaporator temperature. The maximum range of the evaporator temperature is about 11 K at different angles and heat inputs. Because the LHP was in horizontal position in y - z direction ($\gamma = 0^\circ$), there are only gravitational based pressure losses inside the meander like condenser section. The position of the interface influences the pressure losses in the condenser section which affects the evaporator temperature. The meander like section has only three bends with large radii of curvature and therefore does almost not influence the evaporator temperature.

In comparison to Figure 7, Figure 9 shows slightly higher evaporator temperatures at a higher ambient and coolant temperature of 55°C at different angles γ . When the heat sink temperature increases, the operating temperature of the LHP increases too, leading to an increase of the evaporator wall temperature. The coolant flow was fixed to $0.14 \text{ m}^3/\text{h}$. While the evaporator temperatures for angles $\gamma \geq 0^\circ$ (evaporator above condenser) differ very little with variable heat input, there are fluctuations in evaporator temperatures for negative angles. This could be due to bubble generation inside the reservoir that results in pressure fluctuations in the LHP.

4.2 Evaporator temperature difference

As shown in Figure 5 two temperature sensors are attached to the evaporator. One is placed between heat source and evaporator top (position $Evap_1$). The other one is attached below the evaporator (position $Evap_2$). The temperature difference between these two positions is defined as:

$$\Delta T_{Evap} = T_{Evap_1} - T_{Evap_2} \quad (2)$$

As it can be seen in Figure 10 the temperature difference ΔT_{Evap} ranges from 0.4 to 3.0 K at ambient and coolant temperatures of 20 °C. The values for positive angles are smaller than for negative angles. For positive angles a slight increase of ΔT_{Evap} can be observed as the heat load is increased. The slopes of the curves are greater for low heat loads than for higher heat loads. That means an increase of effective heat conductivity through the porous medium along the temperature sensor axis that could result from a decreasing vapour layer thickness inside the porous medium and/or higher mass flow rates with increasing heat loads.

The temperature differences ΔT_{Evap} for negative angles are higher than those at positive angles for heat loads ranging from 20 W to 60 W. This results from lower effective heat conductivities along the temperature sensor axis that could be affected by thicker vapour layers inside the porous medium. At negative angles the compensation chamber is located below the evaporator, which hinders the working fluid supply to the evaporator. As the heat load is further increased, the interface inside the condenser moves toward the compensation chamber and allows an efficient working fluid supply to the porous medium. Then the vapour layer becomes thinner and the temperature difference ΔT_{Evap} reaches the same level as for positive angles.

Figure 11 shows the temperature difference ΔT_{Evap} for ambient and coolant temperatures of 55 °C, which ranges from 1.7 K to 5.25 K. This higher temperature differences in comparison to Figure 10 could result from thicker vapour layers inside the porous media. There are also smaller temperature differences for positive angles than for negative angles. The temperature

difference ΔT_{Evap} for positive angles does not increase as much as at ambient and coolant temperatures of 20 °C. For an angle of 0°, the temperature difference ΔT_{Evap} could even be assumed constant. That very slightly increase of the temperature difference ΔT_{Evap} means a big increase in effective heat conductivity along the temperature sensor axis.

As also seen in Figure 10 the temperature difference ΔT_{Evap} at negative angles does not follow any systematic behaviour. The interaction of the position of the interface inside the condenser, the orientation and the position of the compensation chamber are very complex and needs to be further investigated.

4.3 Temperature distribution along the LHP

Figure 12a) and Figure 12b) show the temperature distributions along the LHP from position *Evap_1* to position *CC* at ambient and coolant temperatures of 20 °C for heat loads of 20 W and 100 W, respectively. As soon as the vapour enters the condenser, it condenses and the liquid reaches the coolant temperature. Even at the condenser inlet (*HS_1*), the temperatures at 20 W are around 20 °C. For a heat load of 100 W, the temperatures begin to increase from position *LL3* instead of *LL2* for 20 W, showing that the interface inside the condenser is shifted toward the liquid line. The desuperheating length has increased too, since for a heat load of 20 W, the temperature at position *HS_1* reaches the coolant temperature, but at the maximum heat load of 100 W, the temperature reaches the coolant temperature at a posterior position (except for the 60° angle).

The temperature level at the angle of 60° is higher than that at 90°, due to the lower coolant flow rate (see section 4.1).

Figure 13a) and Figure 13b) show the temperature distribution along the LHP from position *Evap_1* to position *CC* at ambient and coolant temperature of 55 °C for heat loads of 20 W and

100 W, respectively. The same behaviour of the temperature trend as in Figure 12 can be observed. The confused temperature levels at different angles do not result from a coolant flow rate variation, which was fixed to a constant value of 0.14 m³/h. There may be more complex reasons resulting from the position of the interface inside the condenser, the angle γ and the position of the compensation chamber relative to the evaporator that influences the working fluid supply to the porous medium.

4.4 Thermal resistance

The thermal resistance of the evaporator $R_{th,evap}$ is calculated as:

$$R_{th,evap} = \frac{T_W - T_V}{\dot{Q}_{in}} \quad (3)$$

The temperature measured at position Evap_1 in Figure 5 is taken as the evaporator wall temperature T_W while the temperature at position VL_1 is taken as the vapour temperature T_V .

The total thermal resistance of the LHP $R_{th,tot}$ is calculated as:

$$R_{th,tot} = \frac{T_W - T_{sink}}{\dot{Q}_{in}} \quad (4)$$

Here, as well as in equation (3), the temperature measured at position Evap_1 is taken as the evaporator wall temperature T_W , while the heat sink temperature T_{sink} is represented by the mean temperature of the coolant.

Figure 14 shows the thermal resistance of the evaporator for coolant and box ambient temperatures of 20 °C at different angles γ . As the wall and the wicks are highly conductive, the evaporator thermal resistance is very low. For positive angles and horizontal position, the thermal resistance of the evaporator is lower or equal to 0.05 K/W over the whole range of heat load. But for negative angles γ the thermal resistance of the evaporator reaches a maximum value of 0.16 K/W for the lowest heat input of around 20 W (1.25 W/cm²). For higher heat

inputs the thermal resistance decreases down to 0.03 K/W, which is the minimum thermal resistance for all different angles γ at high heat loads. The slightly higher thermal resistances of the evaporator at low heat loads and negative angles γ results from a higher temperature difference between the evaporator wall and the vapour. For positive angles γ , this temperature difference increases with increasing heat load but for positive angles, it decreases. The thermal resistance is linked to the position of the liquid-vapour interface inside the porous medium. High temperature differences are due to low equivalent thermal conductivity, which is typical of pores filled by vapour instead of liquid. This means that the porous medium is not fully saturated and the interface lies inside the porous medium. When the angle γ is negative, the working fluid inside the compensation chamber medium has to flow upward. Especially at low heat loads, as the mass flux is low, the wetting of the porous medium is more difficult than at higher heat fluxes because a larger part of the fluid fill charge is located in the condenser, resulting in a low liquid level in the compensation chamber. Hence, the evaporator thermal resistance is higher.

The total thermal resistance of the LHP for coolant and box ambient temperatures of 20 °C at different angles γ is shown in Figure 15. It shows typical trends for LHPs as shown by other authors [13], [10], [23]. For all angles γ ; the total thermal resistances are characterized by a highly negative slope at low heat loads followed by a gentle decrease with increasing heat load. The increasing heat loads lead to a larger part of the heat transfer surface area of the condenser used for condensation, then to a decrease of the condenser thermal resistance. This results in the decrease of the LHP total thermal resistance. Since the slope of total thermal resistance is not positive at any heat load no dry out of the wick structure appears and hence no crisis of LHP is observed. In addition, the LHP is much more sensitive to the elevation at low heat loads. This is because the mass flow rate is smaller than at higher heat loads and consequently, the frictional

pressure drops are lower too. Hence, the effect of the gravitational pressure drops is much more important with respect to the frictional pressure drops.

The trends show higher total thermal resistances for positive angles than for negative angles γ . The higher total thermal resistances for positive angles result from additional hydrostatic pressure difference to overcome for the working fluid in the liquid line. The maximum total thermal resistance of 2.7 K/W is reached at a heat load of about 20 W (1.25 W/cm²) for angle γ equal to +60°. The minimum total thermal resistance of 0.8 K/W at the same heat load is reached for an angle γ equal to -90°. The minimum total resistance at all angles γ , which ranges from 0.25 to 0.5 W/K, is reached at the maximum heat load of about 100 W (6.25 W/cm²).

Comparing Figure 14 and Figure 15, one notice that the thermal resistance is higher at positive inclination, but the evaporator resistance is lower. This means that the condenser thermal resistance is much higher at positive inclination due to additional gravitational pressure drops in the liquid line.

The maximum total thermal resistance at an angle of γ equal to 60° results from the minimum coolant flow, which is smaller than for other inclinations. When the coolant flow rate is small, the convective heat transfer coefficient between the external wall of the condenser and the coolant fluid is low, leading to an increase of the condenser thermal resistance, hence to an increase of the LHP thermal resistance. It was 0.03 m³/h for 60°, 0.09 m³/h for 0° and 30° and 0.12 m³/h for the other angles (-90°, -60°, -30°, +90°). The variation of coolant flow occurred due to technical reasons.

Figure 16 shows the evaporator thermal resistance for coolant and box ambient temperature of 55 °C at different angles γ . The trends are similar to those at coolant and ambient temperature equal to 20 °C as it can be seen in Figure 14. At positive angles γ , the thermal resistance is very low and almost constant. Negative angles yield to higher evaporator thermal resistances ranging from 1.6×10^{-3} K/W to a maximum of 0.13 K/W at a heat load of around 20 W (1.25 W/cm²).

The evaporator thermal resistance ranges from 16×10^{-3} K/W to 31×10^{-3} K/W at a maximum heat load of 100 W (6.25 W/cm^2) for all angles γ . The slightly negative thermal resistances of around -8×10^{-3} K/W indicated on the chart are not of any physical meaning but result from measurement uncertainties of the temperature and the heat load.

As shown in Figure 17, the total thermal resistances of the LHP for coolant and box ambient temperature of $55 \text{ }^\circ\text{C}$ at different angles γ show trends similar to the total resistances for coolant and ambient temperatures of $20 \text{ }^\circ\text{C}$, but they are slightly lower. This results from the trend of the water saturation curve (p-T- diagram) that shows a higher dp/dT slope at higher temperature level. The decrease of the total thermal resistance with increased coolant temperature was also observed by Maydanik et al. [23] and Chen et al. []. It also needs to be mentioned that the coolant flow rate was increased to $0.14 \text{ m}^3/\text{h}$ for all angles γ .

For low heat loads of around 20 W (1.25 W/cm^2) the total thermal resistance ranges from 0.8 to 1.8 K/W. But for maximum heat loads of around 100 W (6.25 W/cm^2) it ranges from 0.2 to 0.3 K/W.

5. Conclusion

This article investigates the behaviour of a flat-oval evaporator LHP whose overall performance has been analysed experimentally. It was originally designed for electronic cooling in aircrafts, but the necessity to control the LHP boundary conditions has led to test it in a quite different configuration (type of condenser cooling, thermal insulation) than in the real application. The experimental parameters and their variation range are representative of the specifications for aeronautics. The main conclusions are the following:

- The evaporator wall temperatures are higher at positive elevations (evaporator placed above the condenser) and less sensitive to the heat load level than at negative elevations.

- The rotation of the LHP around its longitudinal axis has a low effect on its performances.
- At heat sink and ambient temperature of 55 °C, the evaporator wall temperature is higher than at a heat sink and ambient temperature of 20 °C.
- When the heat sink and ambient temperatures increases to 55 °C, the evaporator wall temperature exhibits great fluctuations at negative elevations, and may exceed the limit allowed for the electronic components.
- The evaporator temperature difference ranges from 0.4 to 3.0 K for heat sink and ambient temperatures of 20 °C and ranges from 1.7 to 5.25 K for heat sink and ambient temperatures of 55 °C.
- For heat sink and ambient temperatures of 20 °C as well as for heat sink and ambient temperatures of 55 °C, the temperature at position *HS_1* reaches the respective heat sink temperatures for a heat load of 20 W. For higher heat loads, the heat sink temperature is reached at a posterior position, showing an increase of the desuperheating length.
- The evaporator thermal resistance is low, particularly at positive elevations. At negative elevations, it is sensitive to operating conditions.
- The LHP total thermal resistance is governed by the heat transfer at the condenser. It decreases with increasing heat load, whatever the operating conditions, because the part of the condenser internal surface area used for condensation increases too.
- The minimum thermal resistance, achieved for a heat load of 100 W (6.25 W/cm²), is of 0.2 K/W. And the maximum thermal resistance with 2.7 K/W is reached at a heat load of 20 W (1.25 W/cm²).

Acknowledgments

This work was conducted in the frame of the European Project "COSEE" (Cooling of Seat Electronic Box and Cabin Equipment"), funded by the European Commission (Contract N° AST5-CT-2006-030800).

References

- [1] Yu.F. Maydanik, Miniature loop heat pipes, 13th IHPC, Shanghai, China, 21-25 Sept. 2004, pp. 23-35.
- [2] W. Zimbeck, G. Slavik, J. Cennamo, S. Kang, J. Yun, E. Kroliczek, Loop heat pipe technology for cooling computer server, 11th Intersociety Conference on Thermal and Thermomechanical Phenomena in Electronic Systems, Orlando (ITHERM 2008), pp. 19-25.
- [3] Yu.F. Maidanik, S.V. Vershinin, M.A. Chernysheva, Evaporative chamber of loop heat pipe, Russian patent # 2170401, 2001.
- [4] Yu.F. Maydanik, S.V. Vershinin, M.A. Chernyshova, Development and tests of miniature loop heat pipes with a flat evaporator, in: Proc. of 30th Int. Conference on Environmental Systems and 7th European Symposium on Space Environmental Control Systems, Toulouse, France, 10–13 July 2000, Paper 2000-01-2491.
- [5] Yu.F. Maydanik, S.V. Vershinin, C. Gerhart, Miniature LHPs with a flat and a cylindrical evaporator—which one is better? in: Proc. of Int. Two-Phase Thermal Control Technology Workshop, Noordwijk, The Netherlands, 15–17 September 2003.
- [6] A.A.M. Delil, V. Baturkin, Y. Friedrikhson, Y. Khmelev, S. Zhuk, Experimental results on heat transfer phenomena in miniature loop heat pipe with a flat evaporator, 12th IHPC, Moscow, 19-24 May 2002, p. 8.
- [7] V.G. Pastukhov, Yu.F. Maidanik, S.V. Vershinin, M.A. Korukov, Miniature loop heat pipes for electronics cooling, Applied Thermal Engineering 23 (2003), pp. 1125-1135.

- [8] V.G. Pastukhov, Yu.F. Maidanik, Low-noise cooling system for PC on the base of loop heat pipes, *Applied Thermal Engineering* 27 (2007), pp. 894-901.
- [9] M.C. Tsai, C.S. Yu, S.W. Kang, Flat plate loop heat pipe with a novel evaporator structure, 21st IEEE Semi-Therm Symposium (2005), p. 4.
- [10] W. Joung, T. Yu, J. Lee, Experimental study on the loop heat pipe with a planar bifacial wick structure, *International Journal of Heat and Mass Transfer* 51 (2008), pp. 1573–1581.
- [11] J.H. Boo, W.B. Chung, Thermal performance of a small-scale loop heat pipe with PP wick, 13th IHPC, Shanghai, China, 21-25 Sept. 2004, pp. 259-264.
- [12] R. Singh, A. Akbarzadeh, M. Mochizuki, Y. Saito, T. NGuyen, F. Kiyooka, V. Wuttijumnong, Thermal performance of miniature loop heat pipe operating under different heating modes, *IEEE* (2006), pp. 557-562.
- [13] R. Singh, A. Akbarzadeh, C. Dixon, M. Mochizuki, R.R. Rhiel, Miniature Loop Heat Pipe with flat evaporator for cooling computer CPU, *IEEE Transactions on Components and Packaging Technologies*, 30 (1) (2007), pp. 42-49.
- [14] R. Singh, A. Akbarzadeh, C. Dixon, M. Mochizuki, R.R. Rhiel, Novel design of miniature loop heat pipe evaporator for electronic cooling, *Journal of Heat Transfer* 129 (2007), pp. 1445-1452.
- [15] Fred A.L. Phillips, Non-inverted meniscus loop heat pipe/capillary pumped loop evaporator, US Patent No. 6533029, 2003.
- [16] Yu.F. Maydanik, Evaporator for Heat Pipe, Russian patent No. 2286526, 2006.
- [17] J. Ptacnik, F. Polasek, Present state of heat pipe technology in the Countries of Mutual Economic Assistance, Proceedings of the third International Heat Pipe Symposium -Tsukuba, Japan Association for Heat Pipes, September 12-14, 1988. Edited by Y. Kobayashi, K. Negishi, K. Oshima, p. 23.
- [18] L.L. Vasiliev, Heat Pipe Technology in CIS Countries, Proceedings of the fourth International Heat Pipe Symposium-Tsukuba, Japan Association for Heat Pipes, May 16-18, 1994. Edited by Y. Kobayashi, K. Oshima, and p. 12-24.

- [19] S. Kakaç, A. Pramuanjaroenkij, L. Vasiliev (eds.), *Mini-Micro Fuel Cells: fundamentals and applications*. Springer Science+Bussiness Media B.V., 2008, 422 p.
- [20] X. Tang, Ch. Park, Vibration/Shock-tolerant capillary two-phase loop technology for vehicle thermal control, *Proceedings of 2008 ASME Summer Heat Transfer Conference (HT 2008)*, August 10-14, 2008, Jacksonville, Florida USA.
- [21] V.V. Doktorau, V.V. Maziuk, Miniature loop heat pipes with non-inverted meniscus, VII Minsk International Seminar “Heat Pipes, Heat Pumps, Refrigerators, Power Sources”, Minsk, 8-11 September 2008, pp. 379-383.
- [22] J.H. Li, Loop Heat Pipe, US Patent No. 7347250 B2, Mar 25, 2008.
- [23] Yu.F. Maydanik, S.V. Vershinin, M.A. Korukov, J.M. Ochterbeck, Miniature Loop Heat Pipes - A Promising Means for Cooling Electronics, *IEEE Transactions on Components and Packaging Technologies* 28 (2) (2005), pp. 290-296.
- [24] Y. Chen, M. Groll, R. Mertz, Yu.F. Maydanik, S.V. Vershinin, Steady-state and transient performance of a miniature loop heat pipe, *International Journal of Thermal Sciences* 45 (11) (2006), pp. 1084-1090.

Figure captions

Figure 1 : Frame of the passenger seat and location of the SEB	23
Figure 2 : Evaporator details	24
Figure 3 : LHP – a) with radiator, top view; b) view from below; c) condenser box	25
Figure 4 : Test rig instrumentation – a) sketch, b) photo	26
Figure 5 : Positions of thermocouples.....	27
Figure 6 : LHP – a) front view – angle γ , b) side view – angle δ	28
Figure 7 : Evaporator temperatures at $T_{amb} = 20^{\circ}\text{C}$ and $T_{cool} = 20^{\circ}\text{C}$, variation of γ , LHP isolated	29
Figure 8 : Evaporator temperatures at $T_{amb} = 20^{\circ}\text{C}$ and $T_{cool} = 20^{\circ}\text{C}$, variation of δ , LHP isolated	30
Figure 9 : Evaporator temperatures at $T_{amb} = 55^{\circ}\text{C}$ and $T_{cool} = 55^{\circ}\text{C}$, LHP isolated except heat sink	31
Figure 10 : Temperature difference $\Delta T_{Evap} = T_{Evap_1} - T_{Evap_2}$ at $T_{amb} = 20^{\circ}\text{C}$ and $T_{cool} = 20^{\circ}\text{C}$...	32
Figure 11 : Temperature difference $\Delta T_{Evap} = T_{Evap_1} - T_{Evap_2}$ at $T_{amb} = 55^{\circ}\text{C}$ and $T_{cool} = 55^{\circ}\text{C}$, ..	33
Figure 12 : Temperature distribution along LHP at $T_{amb} = 20^{\circ}\text{C}$ and $T_{cool} = 20^{\circ}\text{C}$, variation of γ ,	34
Figure 13: Temperature distribution along LHP at $T_{amb} = 55^{\circ}\text{C}$ and $T_{cool} = 55^{\circ}\text{C}$, variation of γ ,	35
Figure 14 : Thermal resistance of evaporator at $T_{amb} = 20^{\circ}\text{C}$ and $T_{cool} = 20^{\circ}\text{C}$, variation of γ ...	36
Figure 15 : Total thermal resistance at $T_{amb} = 20^{\circ}\text{C}$ and $T_{cool} = 20^{\circ}\text{C}$, variation of γ	37
Figure 16 : Thermal resistance of evaporator at $T_{amb} = 55^{\circ}\text{C}$ and $T_{cool} = 55^{\circ}\text{C}$, variation of γ ..	38
Figure 17 : Total thermal resistance at $T_{amb} = 55^{\circ}\text{C}$ and $T_{cool} = 55^{\circ}\text{C}$, variation of γ	39

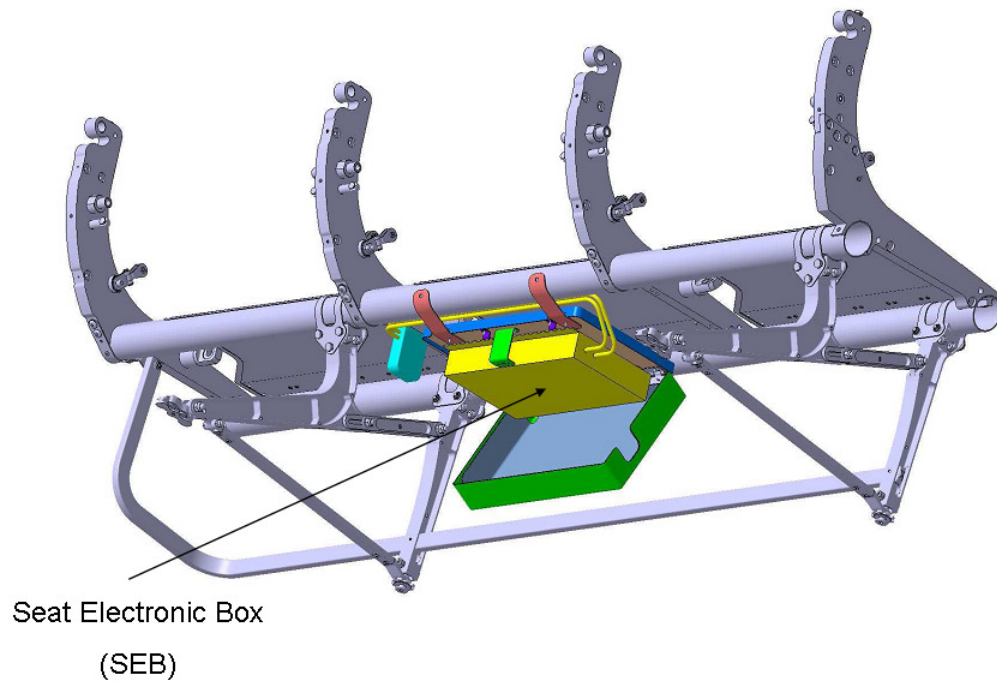


Figure 1: Frame of the passenger seat and location of the SEB

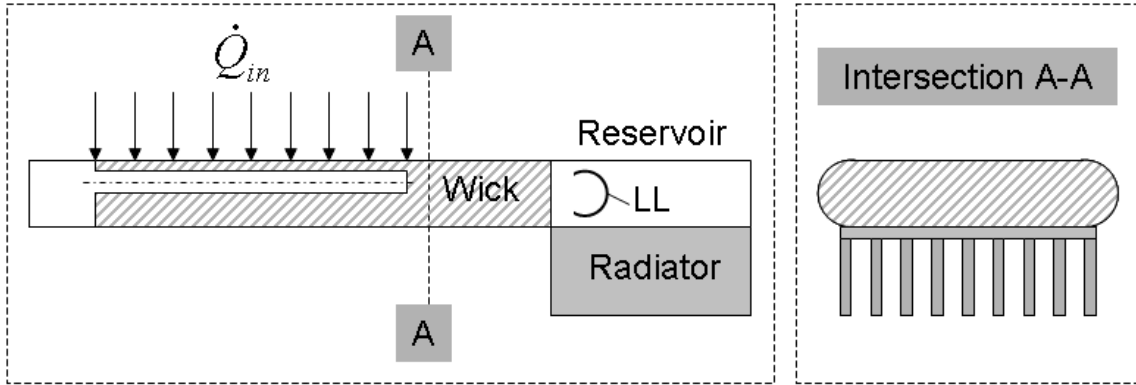


Figure 2 : Evaporator details

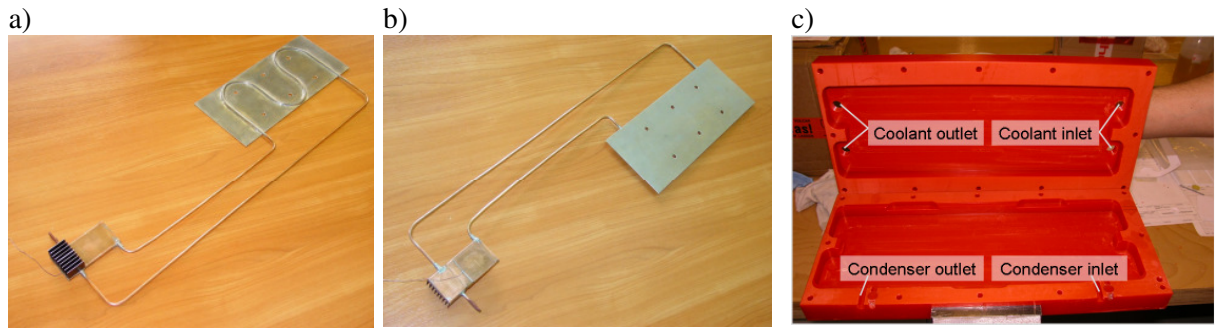


Figure 3 : LHP – a) with radiator, top view; b) view from below; c) condenser box

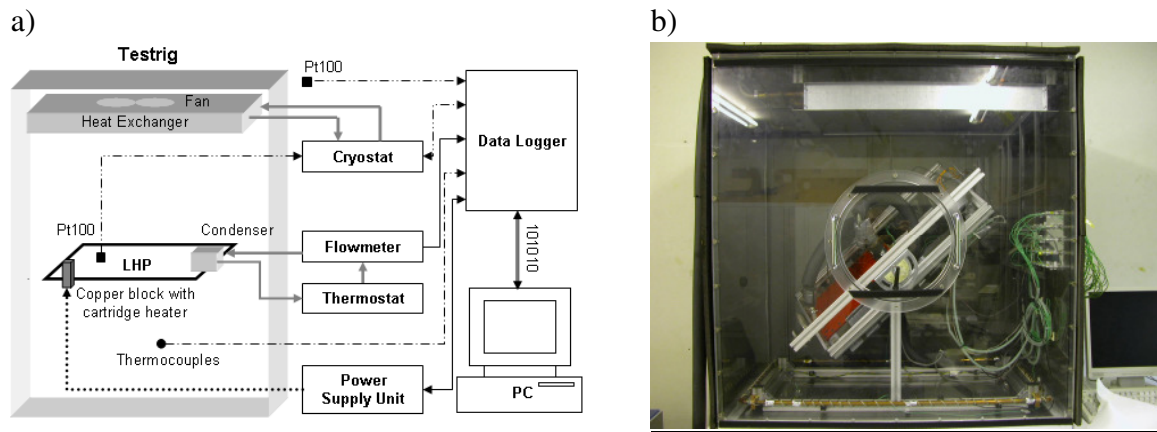


Figure 4 : Test rig instrumentation – a) sketch, b) photo

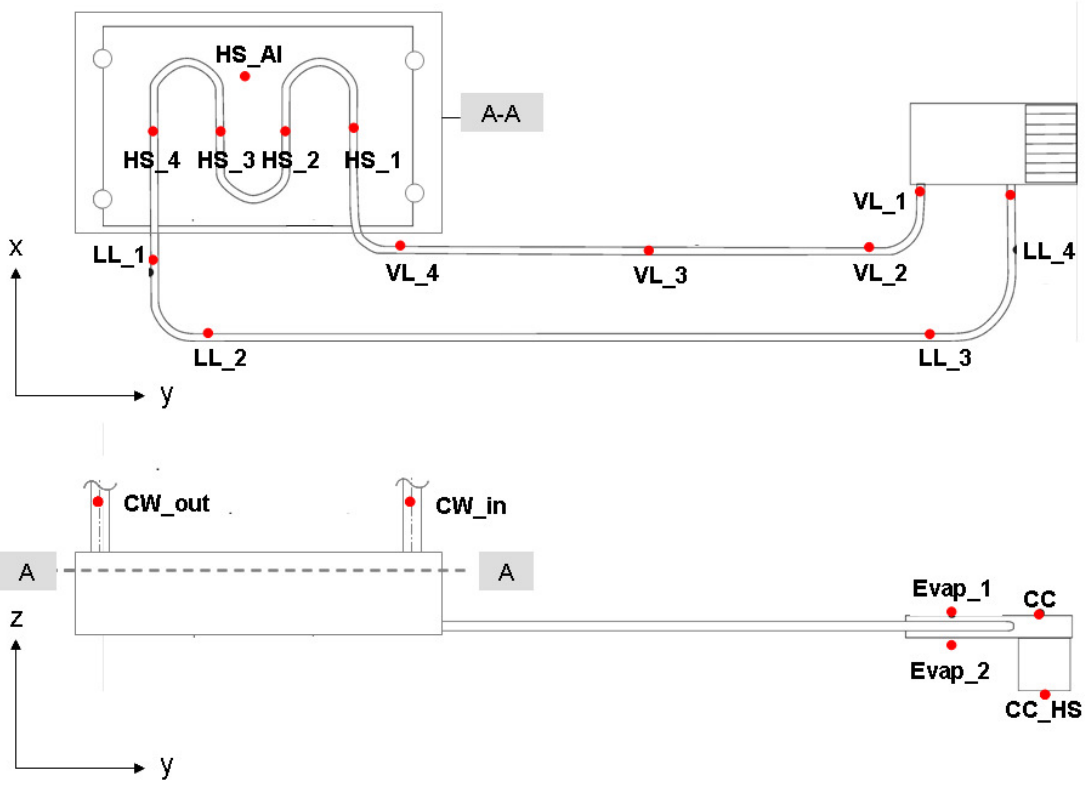
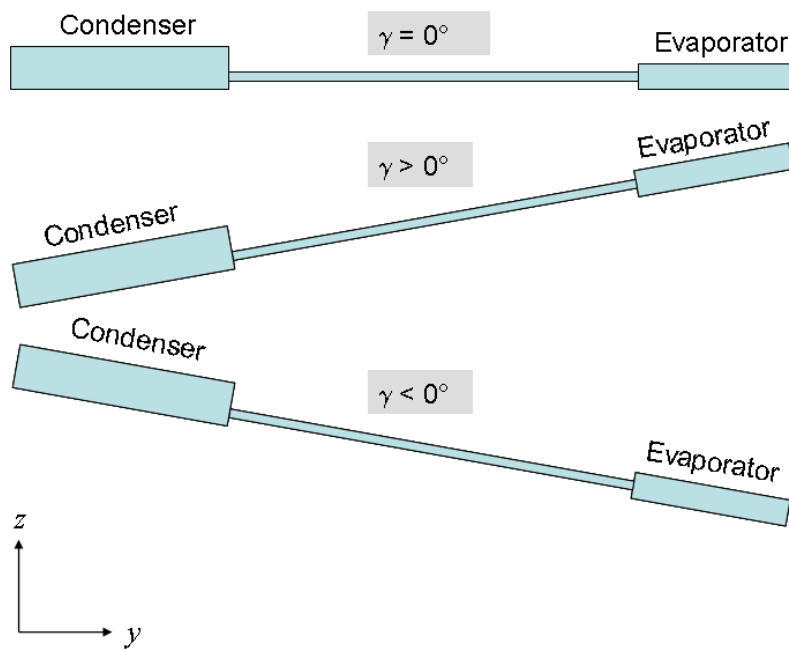


Figure 5 : Positions of thermocouples

a) Front view / angle γ



b) View from right side / angle δ

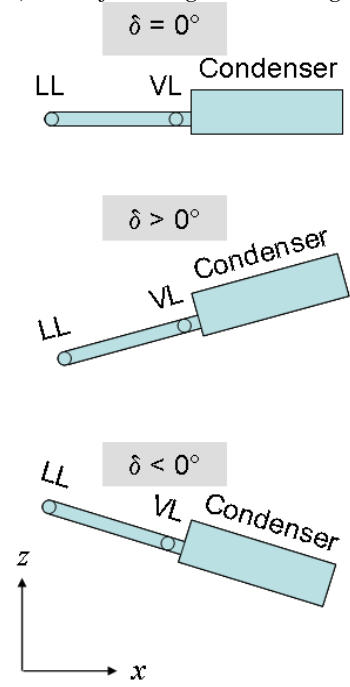


Figure 6 : LHP – a) front view – angle γ ; b) side view – angle δ

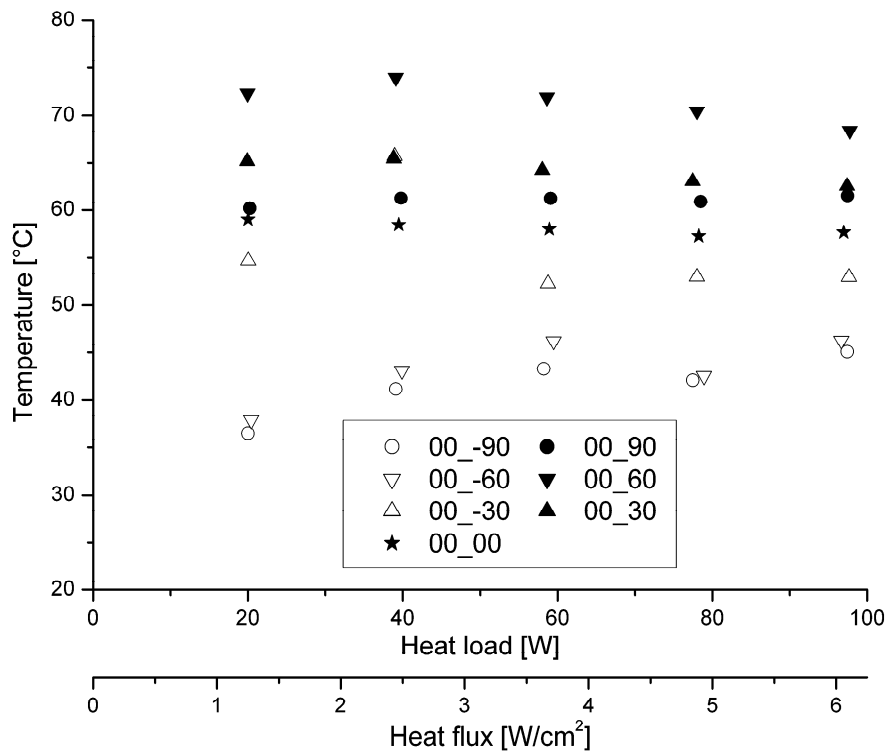


Figure 7 : Evaporator temperatures at $T_{amb} = 20^{\circ}\text{C}$ and $T_{cool} = 20^{\circ}\text{C}$, variation of γ , LHP isolated except heat sink at compensation chamber, variation of γ

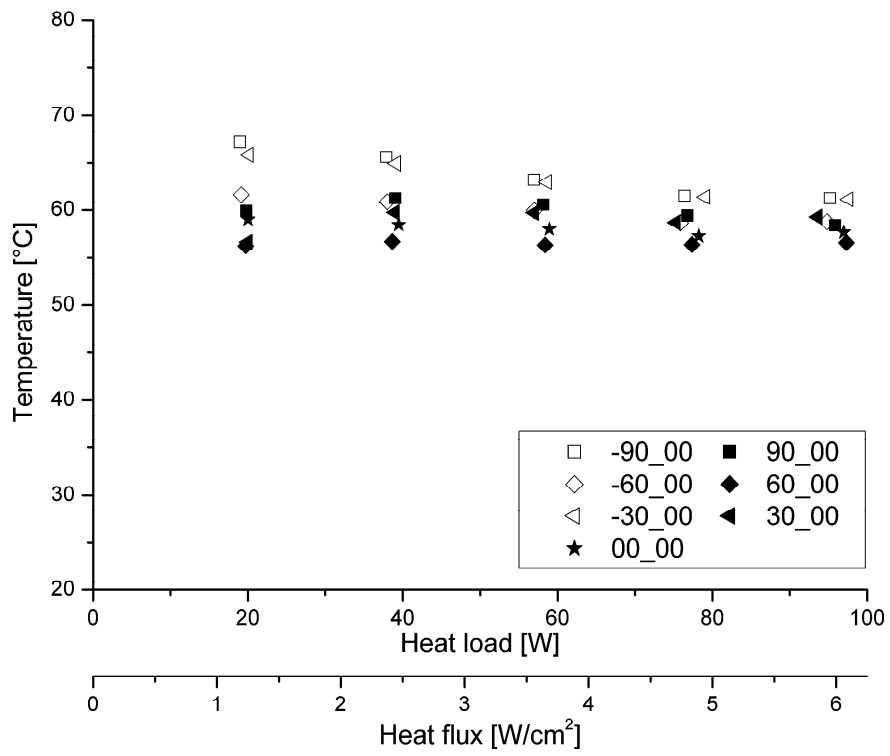


Figure 8 : Evaporator temperatures at $T_{amb} = 20\text{ }^{\circ}\text{C}$ and $T_{cool} = 20\text{ }^{\circ}\text{C}$, variation of δ , LHP isolated except heat sink at compensation chamber

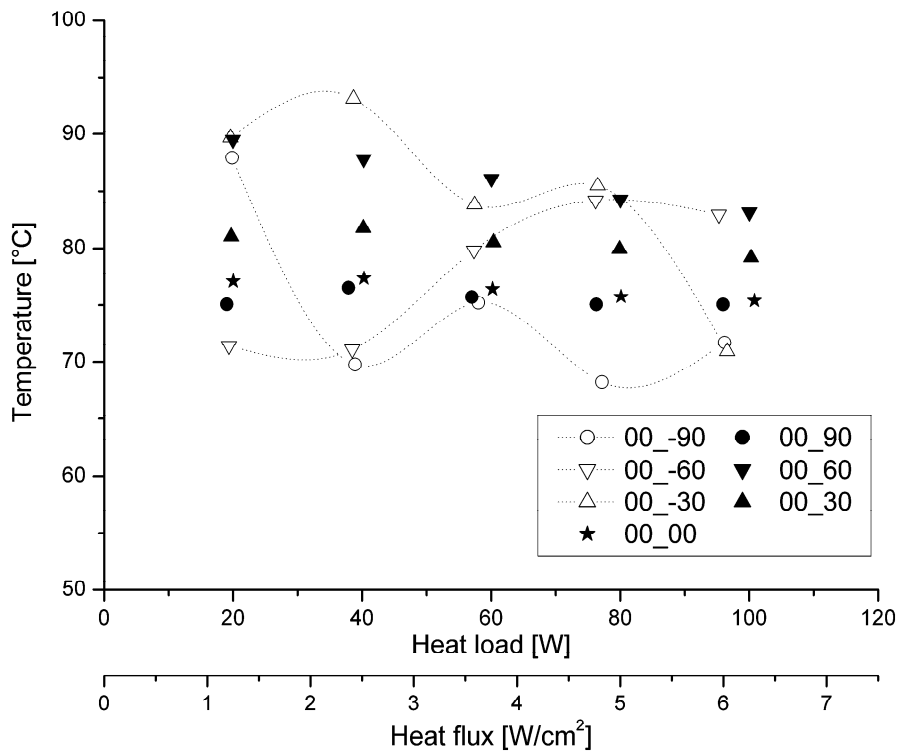


Figure 9 : Evaporator temperatures at $T_{amb} = 55 \text{ }^\circ\text{C}$ and $T_{cool} = 55 \text{ }^\circ\text{C}$, LHP isolated except heat sink at compensation chamber, variation of γ

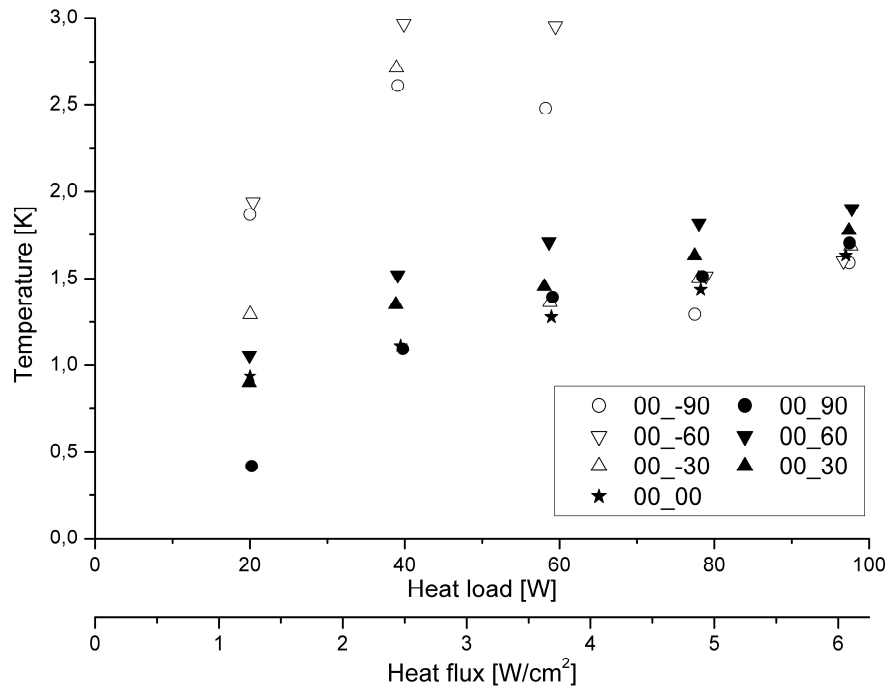


Figure 10 : Temperature difference $\Delta T_{Evap} = T_{Evap_1} - T_{Evap_2}$ at $T_{amb} = 20^{\circ}\text{C}$ and $T_{cool} = 20^{\circ}\text{C}$, LHP isolated, except heat sink at compensation chamber, variation of γ

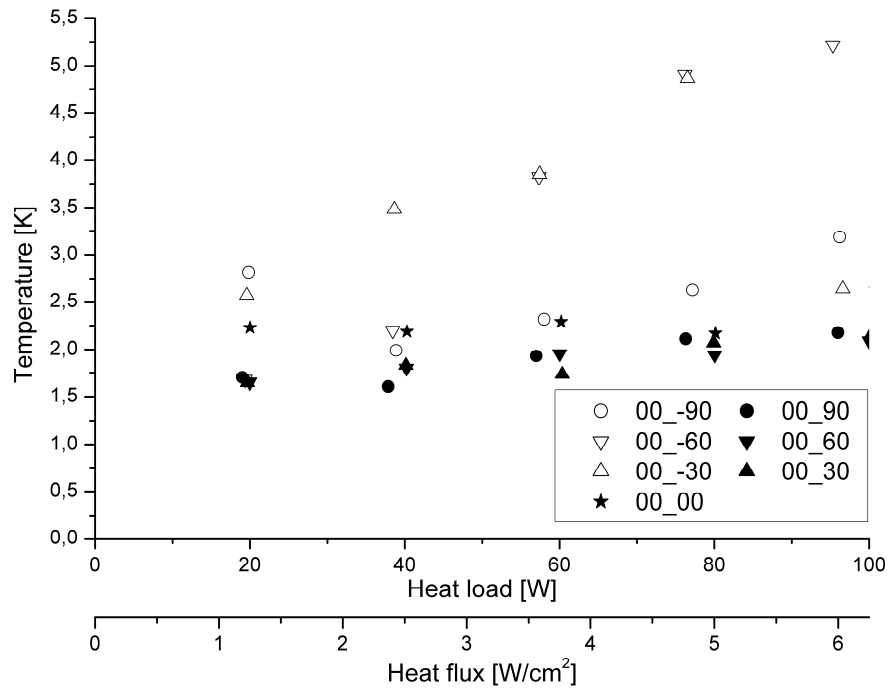
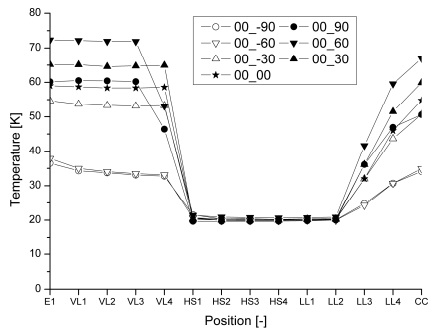
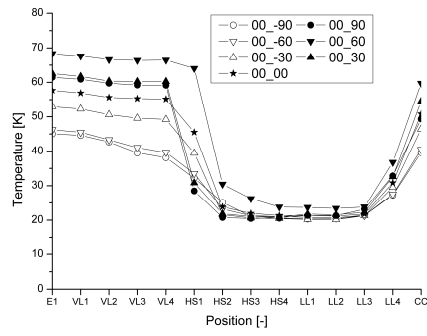


Figure 11 : Temperature difference $\Delta T_{Evap} = T_{Evap_1} - T_{Evap_2}$ at $T_{amb} = 55^{\circ}\text{C}$ and $T_{cool} = 55^{\circ}\text{C}$, LHP isolated, except heat sink at compensation chamber, variation of γ

a)

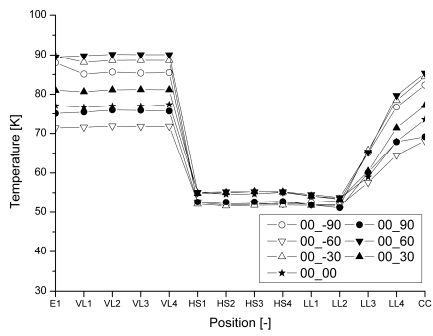


b)



**Figure 12 : Temperature distribution along LHP at $T_{amb} = 20\text{ }^{\circ}\text{C}$ and $T_{cool} = 20\text{ }^{\circ}\text{C}$, variation of γ LHP isolated, except heat sink at compensation chamber,
a) heat load 20 W,
b) heat load 100 W**

a)



b)

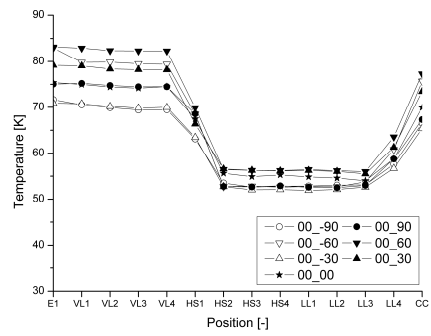


Figure 13: Temperature distribution along LHP at $T_{amb} = 55\text{ }^\circ\text{C}$ and $T_{cool} = 55\text{ }^\circ\text{C}$, variation of γ , LHP isolated, except heat sink at compensation chamber,
a) heat load 20 W,
b) heat load 100 W

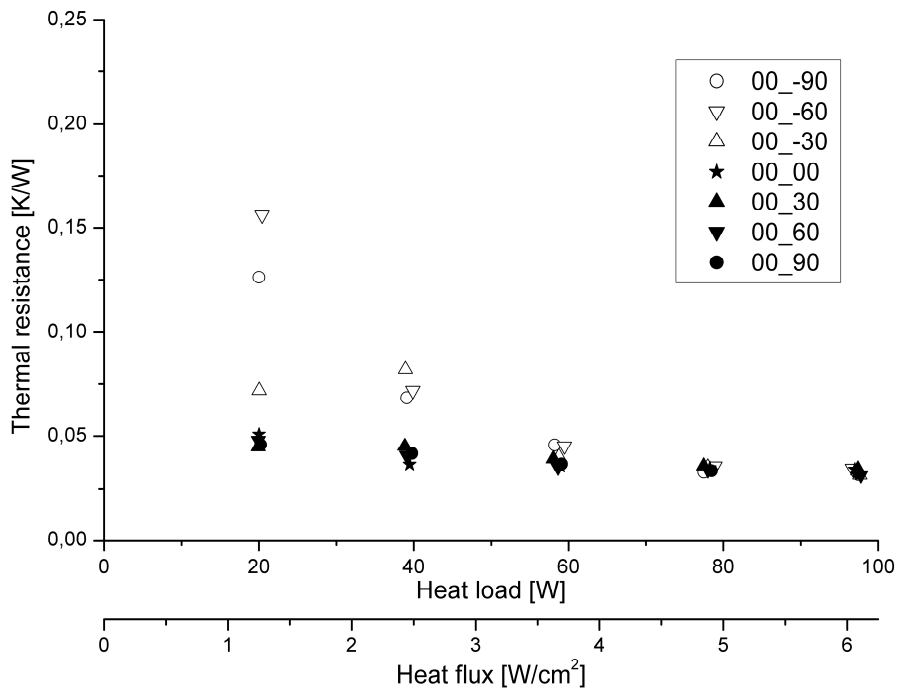


Figure 14 : Thermal resistance of evaporator at $T_{amb} = 20^{\circ}\text{C}$ and $T_{cool} = 20^{\circ}\text{C}$, variation of γ

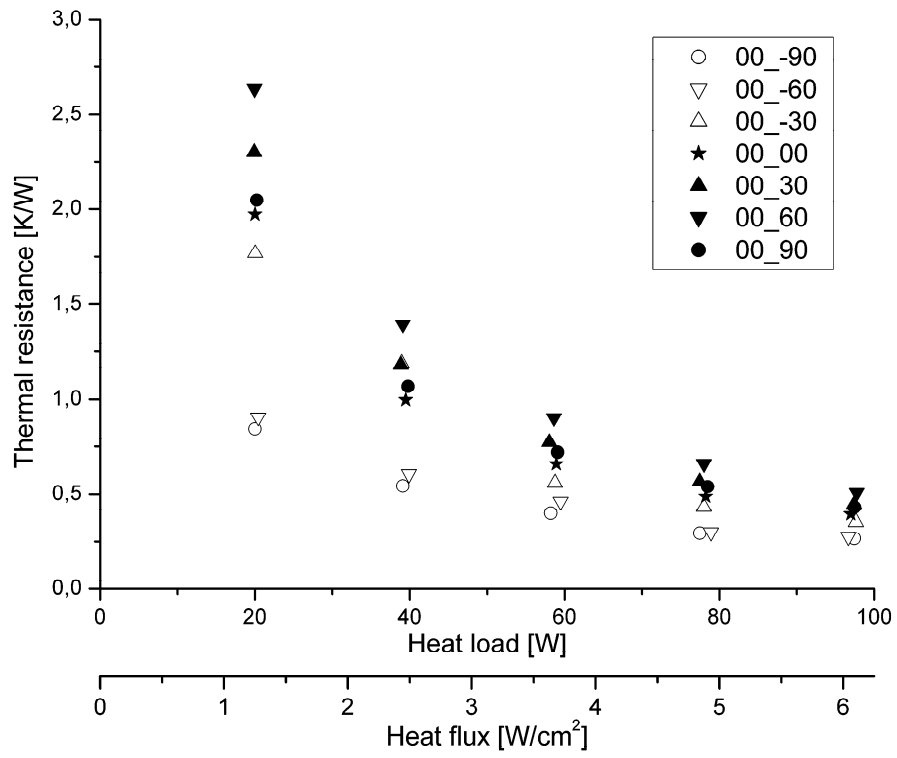


Figure 15 : Total thermal resistance at $T_{amb} = 20^{\circ}\text{C}$ and $T_{cool} = 20^{\circ}\text{C}$, variation of γ

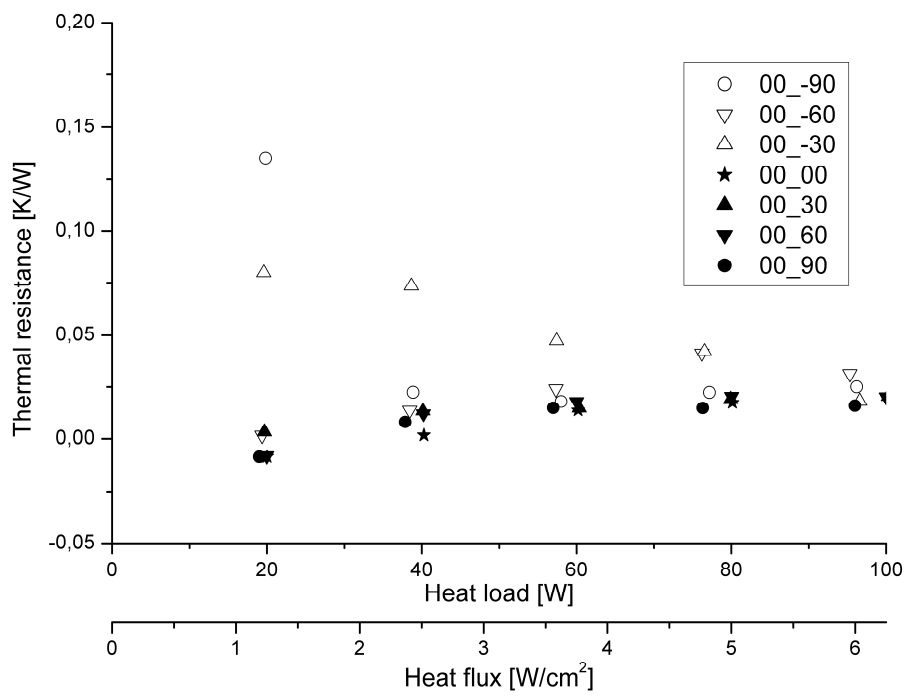


Figure 16 : Thermal resistance of evaporator at $T_{amb} = 55\text{ }^{\circ}\text{C}$ and $T_{cool} = 55\text{ }^{\circ}\text{C}$, variation of γ

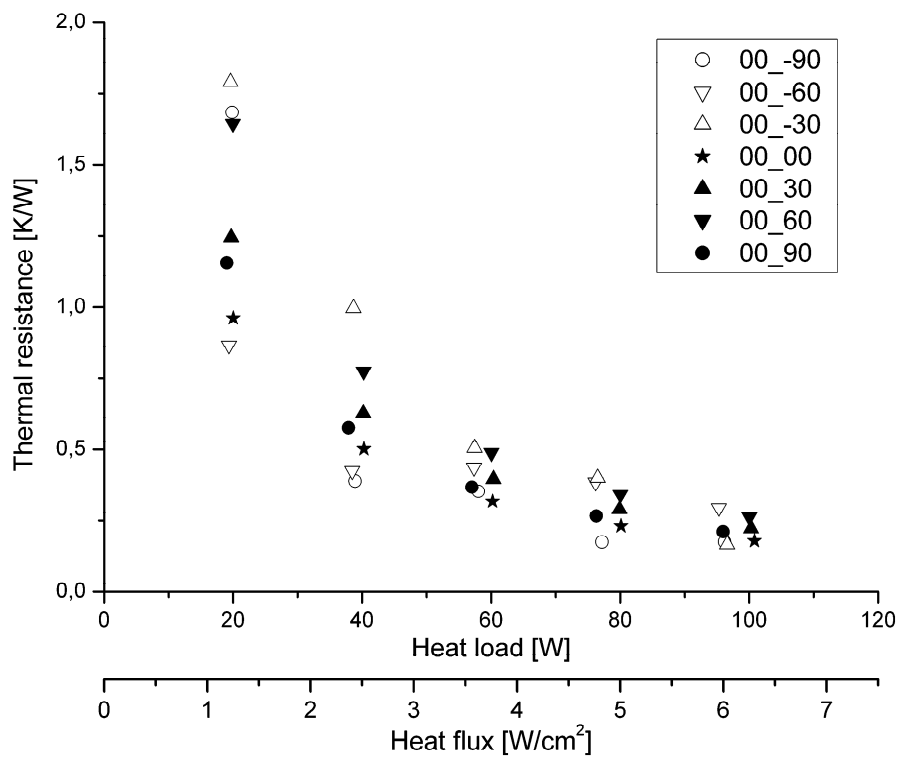


Figure 17 : Total thermal resistance at $T_{amb} = 55\text{ }^{\circ}\text{C}$ and $T_{cool} = 55\text{ }^{\circ}\text{C}$, variation of γ

Evaporator	
Length [mm]	85
Width [mm]	42
Thickness [mm]	7
Body wall thickness [mm]	0.5
Wick	
Length [mm]	55
Porosity [%]	68.8
Pore breakdown radius [μm]	8.0
Compensation chamber	
Length [mm]	20
Vapour line	
Length [mm]	358
Diameter [mm]	4
Liquid line	
Length	765
Diameter	3
Condenser	
Length [mm]	562
Filling volume [cm^3]	19.24

Table 1 : LHP design parameters

Parameter	Variation / explanation
Type of cooling	Forced convection: <ul style="list-style-type: none"> · A condenser is attached to the condenser section with water as a coolant · Insulation along the loop heat pipe except at compensation chamber heat sink
Coolant temperature	$T_{Cool} = \{20;55\}^{\circ}C$
Box ambient temperature	$T_{Box,amb} = \{20;55\}^{\circ}C$
Orientation	Orientation in y-z direction γ <ul style="list-style-type: none"> · evaporator above condenser : positive angles · evaporator under condenser : negative angles · $\gamma = \{-90;-60;-30;0;+30;+60;+90\}^{\circ}$ Orientation in x-z direction δ <ul style="list-style-type: none"> · vapour line above liquid line: positive angle · vapour line under liquid line: negative angle · $\delta = \{-90;-60;-30;0;+30;+60;+90\}^{\circ}$
Power input	Electrical power input P_{el} $P_{el} = \{0;20;40;60;80;100\}W$

Table 2 : Parameter variation

Answers to the reviewer comments

Reviewer#2

The manuscript can be recommended for its further publication in ATE after minor revision. The problems below should be appropriately dealt with:

1. the Introduction section should be shortened.

Answer: The introduction of the initial version of the manuscript has been shortened. But, as the reviewer #3 asked for a literature survey on non-inverted meniscus type LHP evaporators, a supplementary paragraph has been added.

2. the authors should give the detailed temperature distribution along the loop for steady state operation, especially all the temperature readings of the TCs on the evaporator wall, not only one reading of the evaporator temperature.

Answer: Two new chapters have been introduced with the corresponding figures:

4.2 Comparison between evaporator temperatures at position Evap_1 (between heat source and evaporator top) and position Evap_2 (below the evaporator)

4.3 Temperature distribution along the LHP

3. the temperature fluctuation should be given in the form of the graph for the understanding of readers.

Answer: Spline functions have been added to figure 9.

Reviewer#3: Review of the Manuscript Number: ATE-2009-589

S. Becker, S. Vershinin, V. Sartre, E. Laurien, L. Bonjour, Yu. F. Maydanik "Investigation of the copper-water LHP with flat-oval evaporator"

We ought to testify, that the authors in modified option of the manuscript clarified the principle of non-inverted meniscus evaporator operation. Now there is a question about the literature analysis (introduction). If the evaporator is non-inverted, the literature search ought to be oriented on the loop heat pipes with non-inverted meniscus of the evaporation. In such a case the literature search [1-14] has no direct relationship with the manuscript topic. On the contrary, there is a lack of the literature search in the field of non-inverted meniscus of the evaporator in the loop heat pipes and thermosyphons. For example:

1. Khrustalev D., Loop thermosyphons for cooling electronics, Thermacore, Inc., US Patent
2. Maziuk V.V., Doktorau VV., Rak A.L. "Miniature loop heat pipes with non-inverted meniscus concept and treatment, International Journal of Low Carbon Technology, No. 13 - July 2006, pp.228-235
3. Ptacnik.J. Polasek, F., Present state of heat pipe technology in the Countries of Mutual Economic Assistance, Proceedings of the third International Heat Pipe Symposium -Tsukuba, Japan Association for Heat Pipes, September 12-14, 1988. Edited by Y. Kobayashi, K. Negishi, K. Oshima, p. 23.
4. Vasiliev L.L., Heat Pipe Technology in CIS Countries, Proceedings of the fourth International Heat Pipe Symposium-Tsukuba, Japan Association for Heat Pipes, May 16-18, 1994. Edited by Y. Kobayashi, K. Oshima, and p. 12-24.

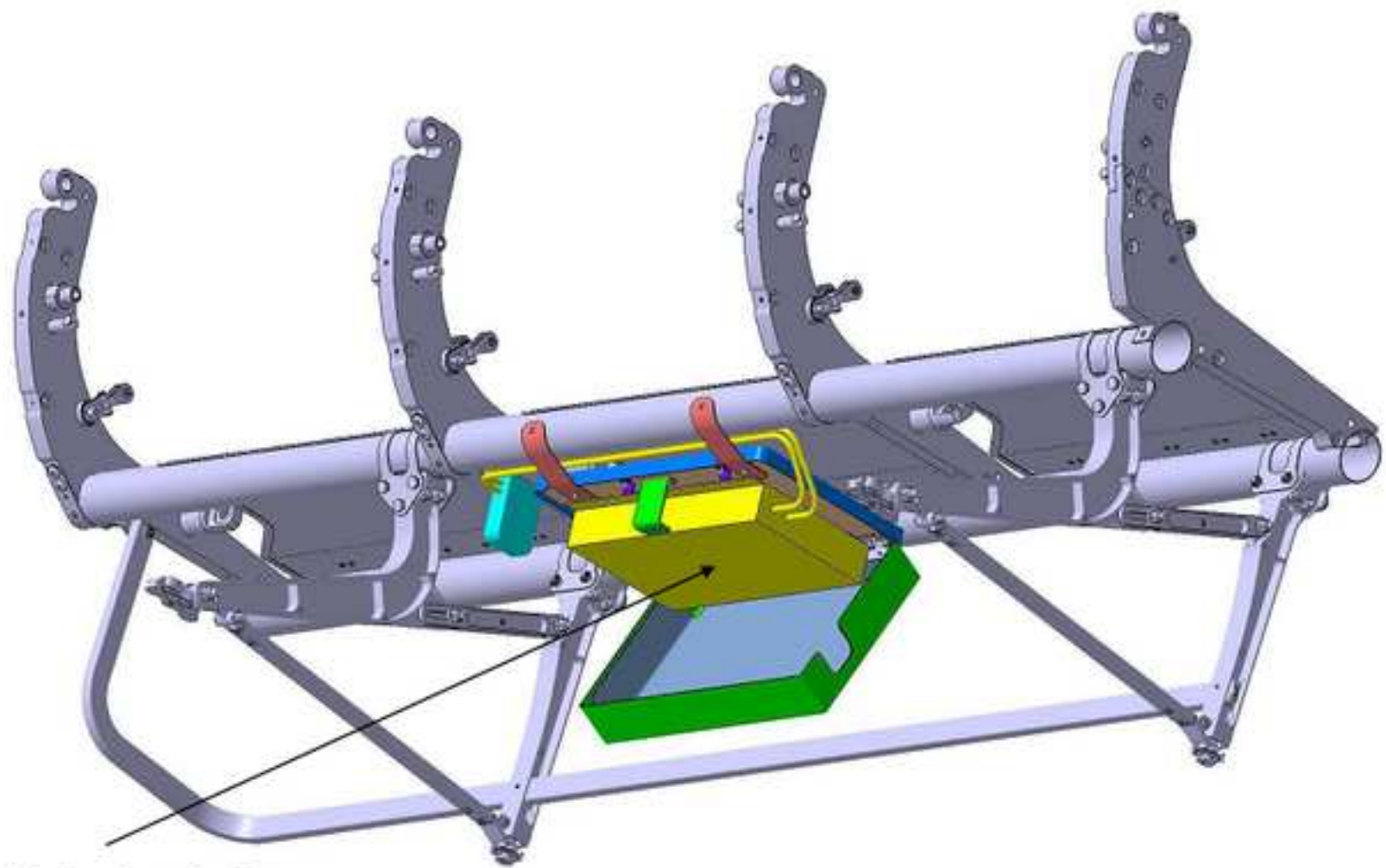
Some former USSR patents (Invention certificates) on this topic were published in the late seventies, early eighteens of the last century (Invention Certificate 587810, BI 1, 1978; Invention Certificate 670790, BI 22, 1979, Invention Certificate 670791, BI 24, 1979; Invention Certificate

870900, BI 37, 1981, Invention Certificate 918677, BI 13, 1982). The topic of these inventions was published in the literature in Russian.

The manuscript can be recommended for its further publication in ATE after the Introduction revision.

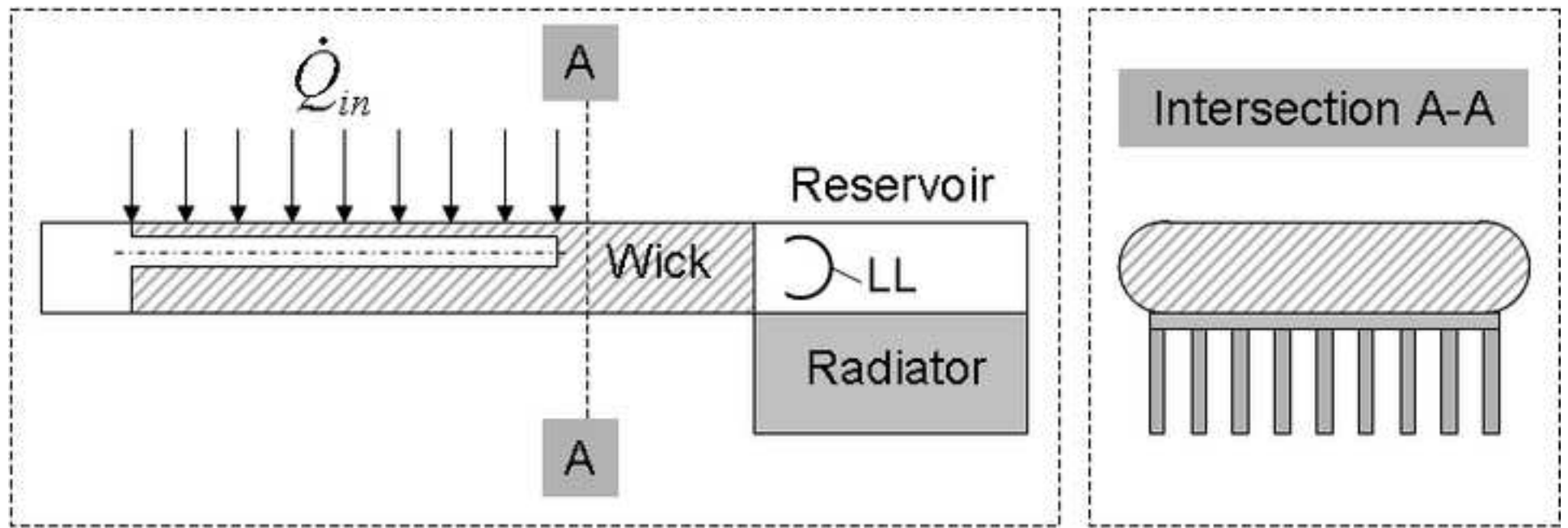
Answer: The authors made an additional literature survey on non-inverted meniscus type evaporators. This research is not exhaustive since this denomination was not always used. The literature study has been modified in order to better clarify this concept and increase the part describing the non-inverted type meniscus LHP evaporators. The USSR patents on this topic were not mentioned in the references, because these patents are not available in English language. The literature survey on LHPs having flat plate evaporators was drastically shortened but not suppressed. As the paper deals with a flat plate evaporator of inverted-meniscus type, authors think that it is of interest to share the literature study in two parts, one dedicated to the flat plate evaporators, the other dedicated to the inverted-meniscus type evaporators, in order to better highlight the originality of the present investigation.

Figure(s)
[Click here to download high resolution image](#)

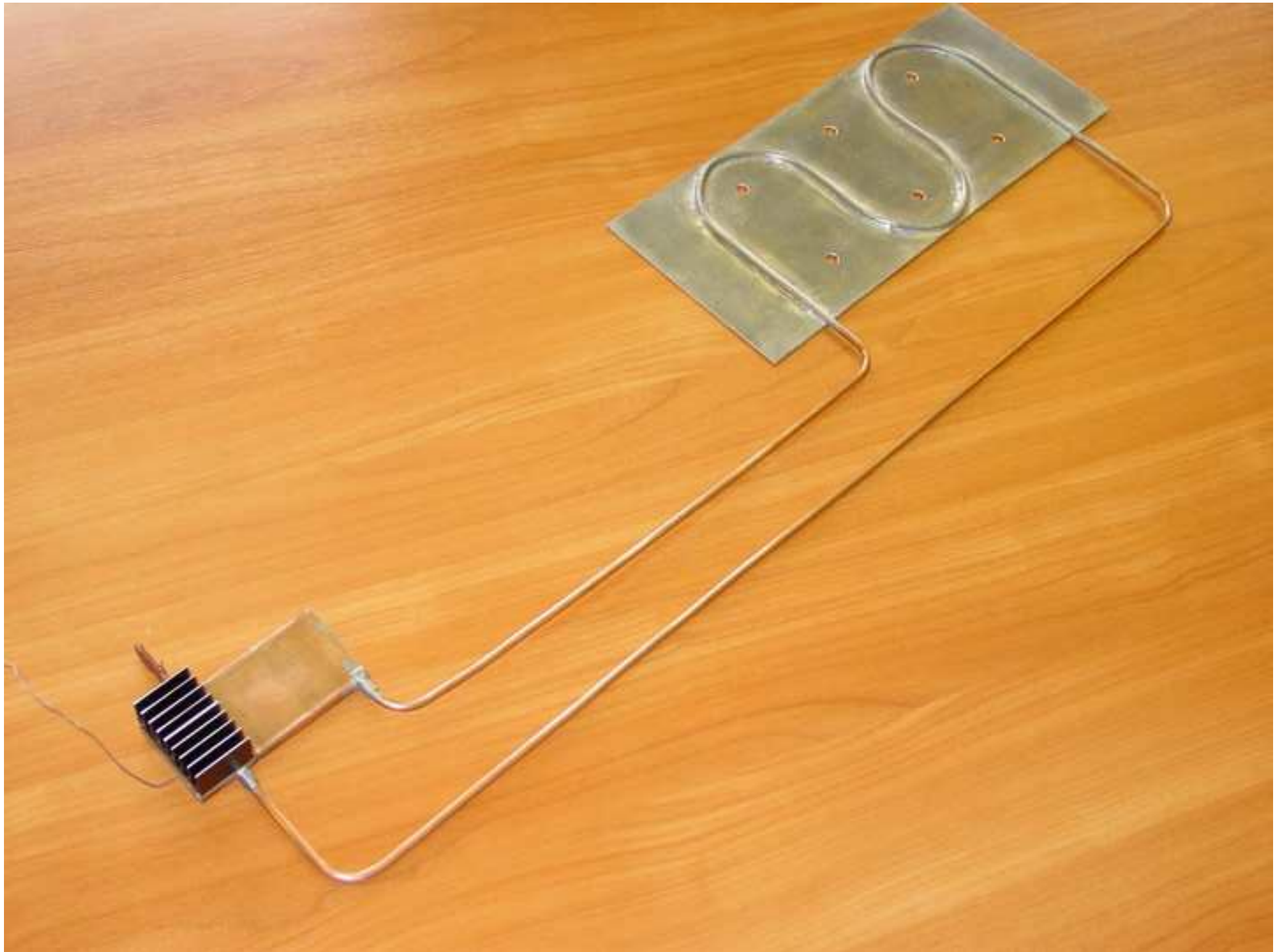


Seat Electronic Box
(SEB)

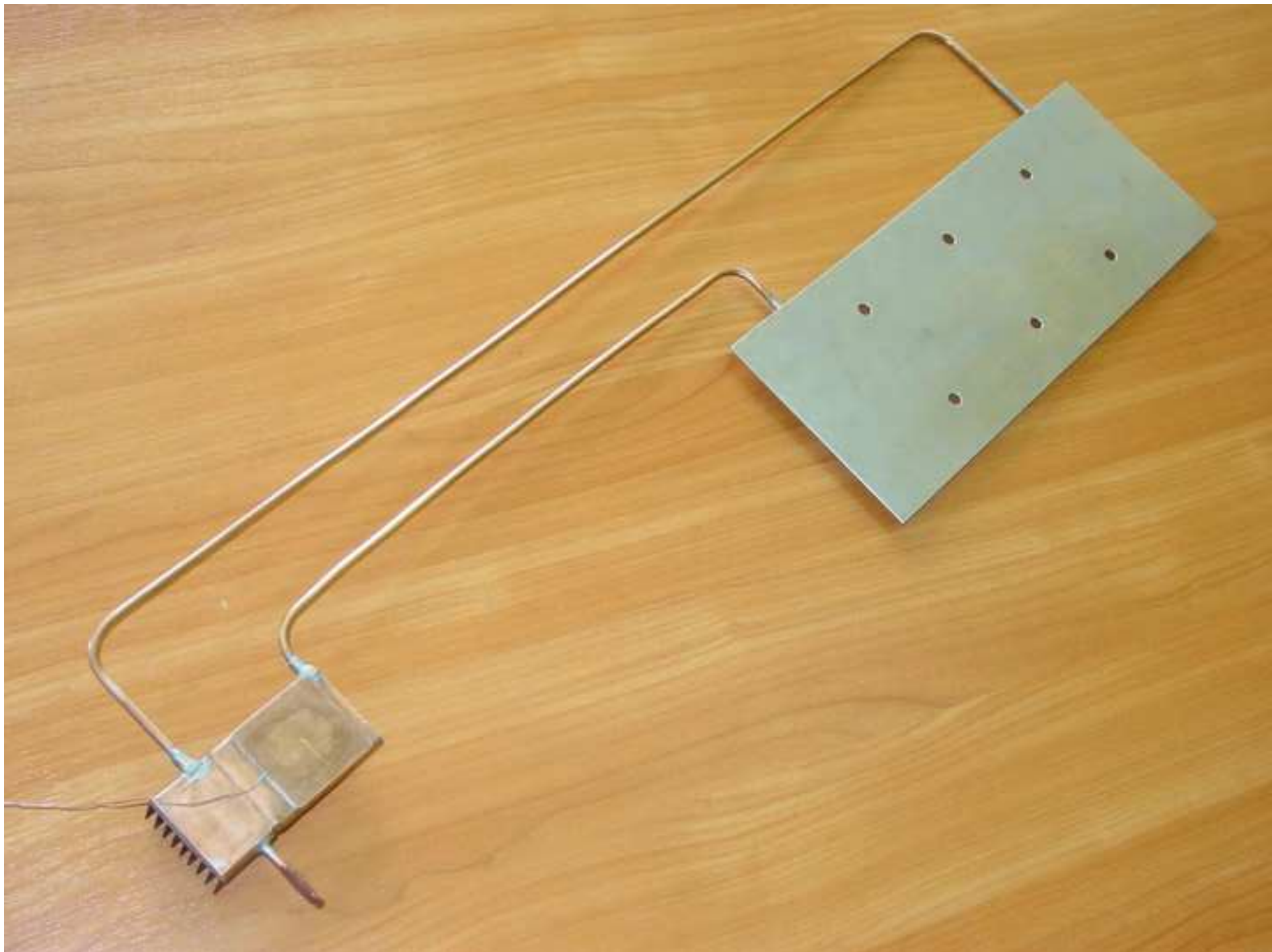
Figure(s)
[Click here to download high resolution image](#)



Figure(s)
[Click here to download high resolution image](#)

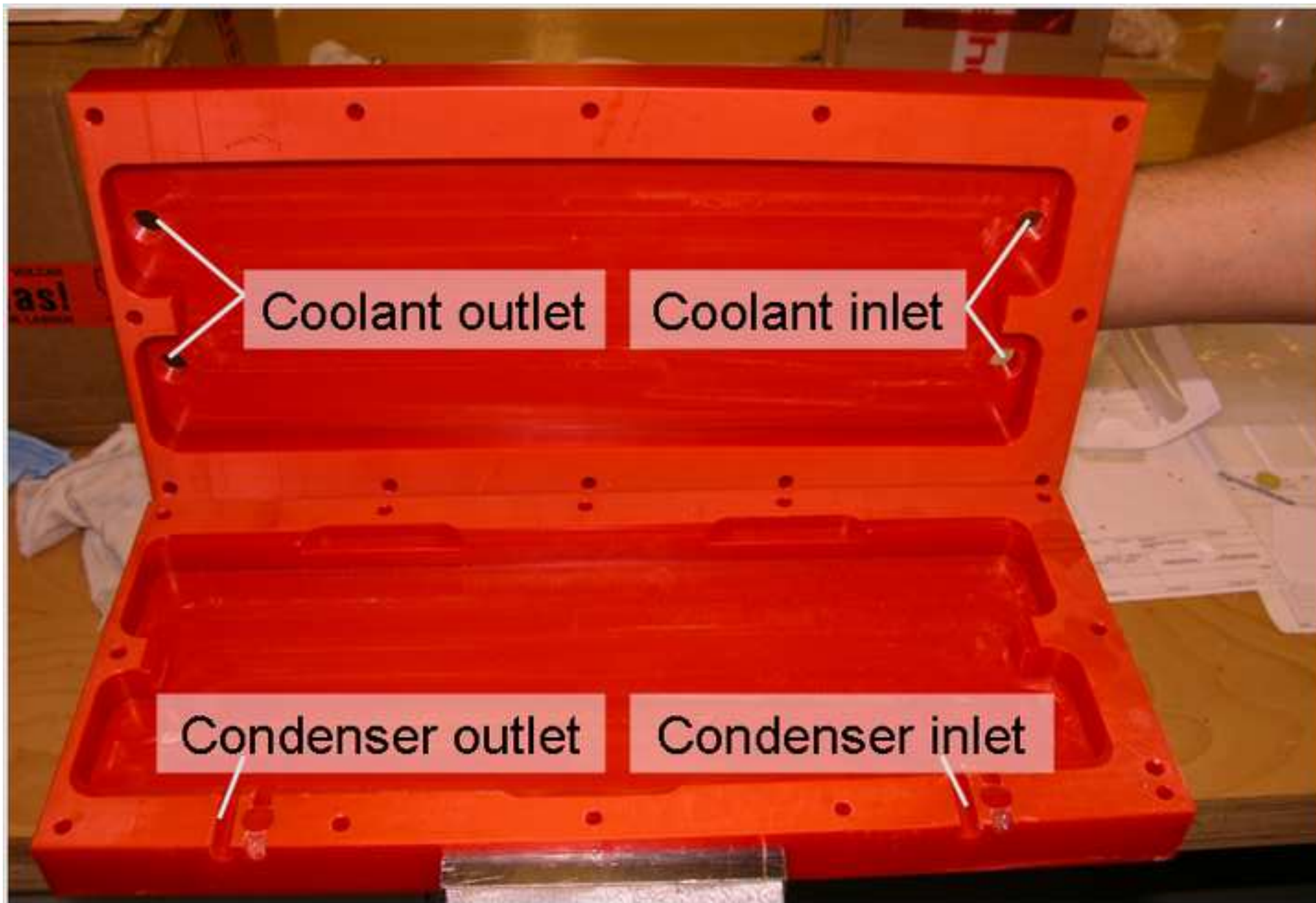


Figure(s)
[Click here to download high resolution image](#)

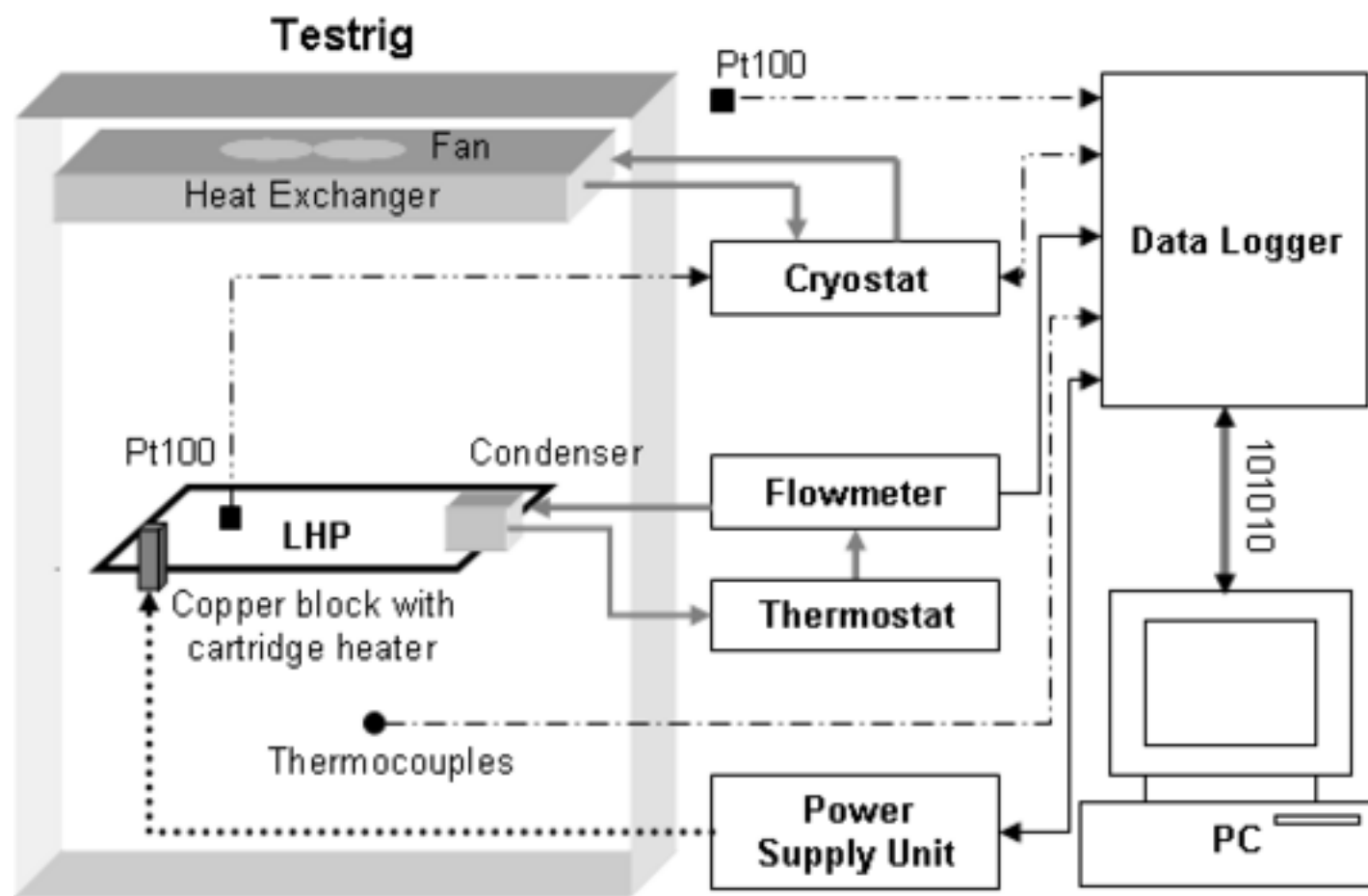


Figure(s)

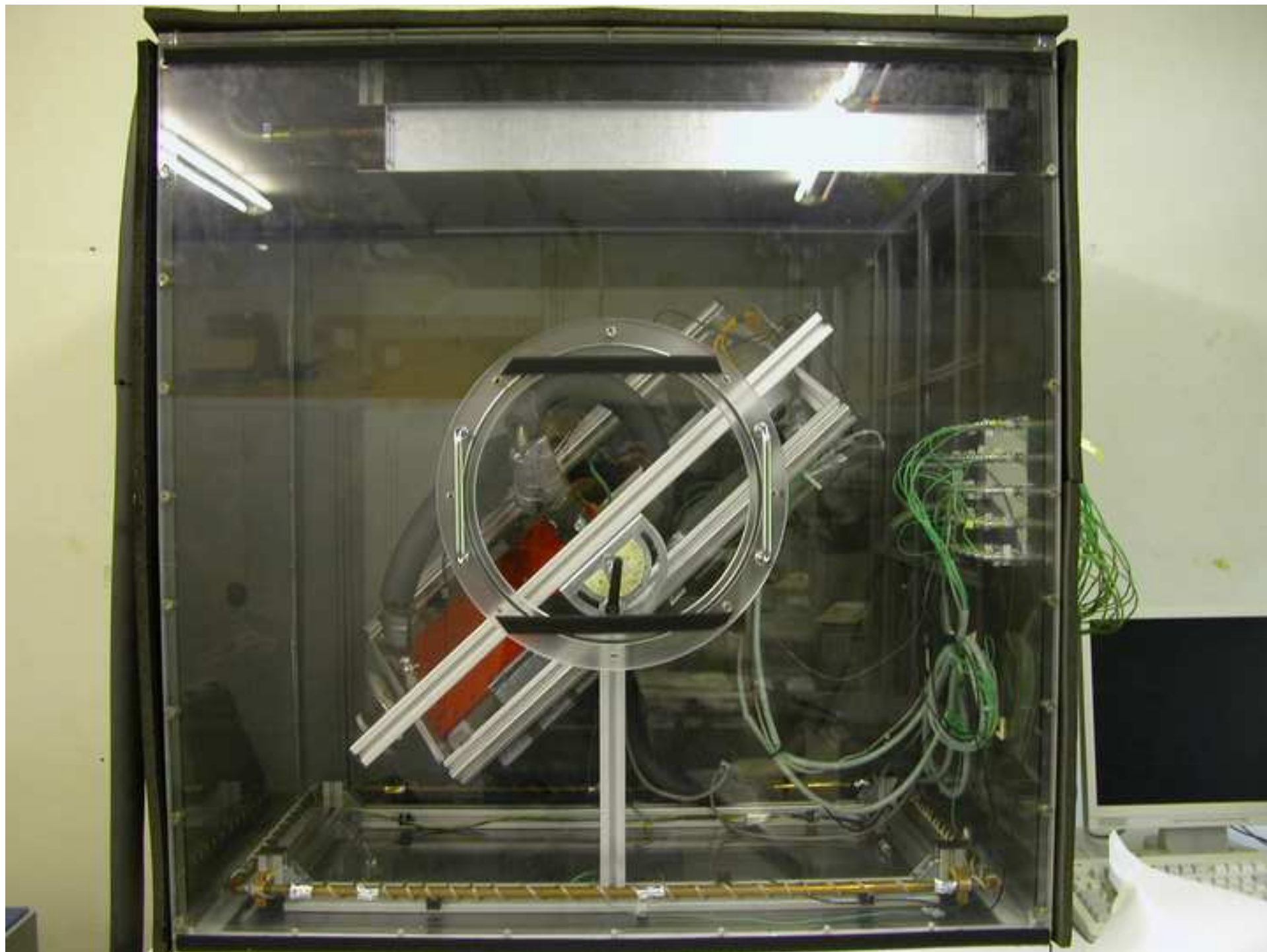
[Click here to download high resolution image](#)



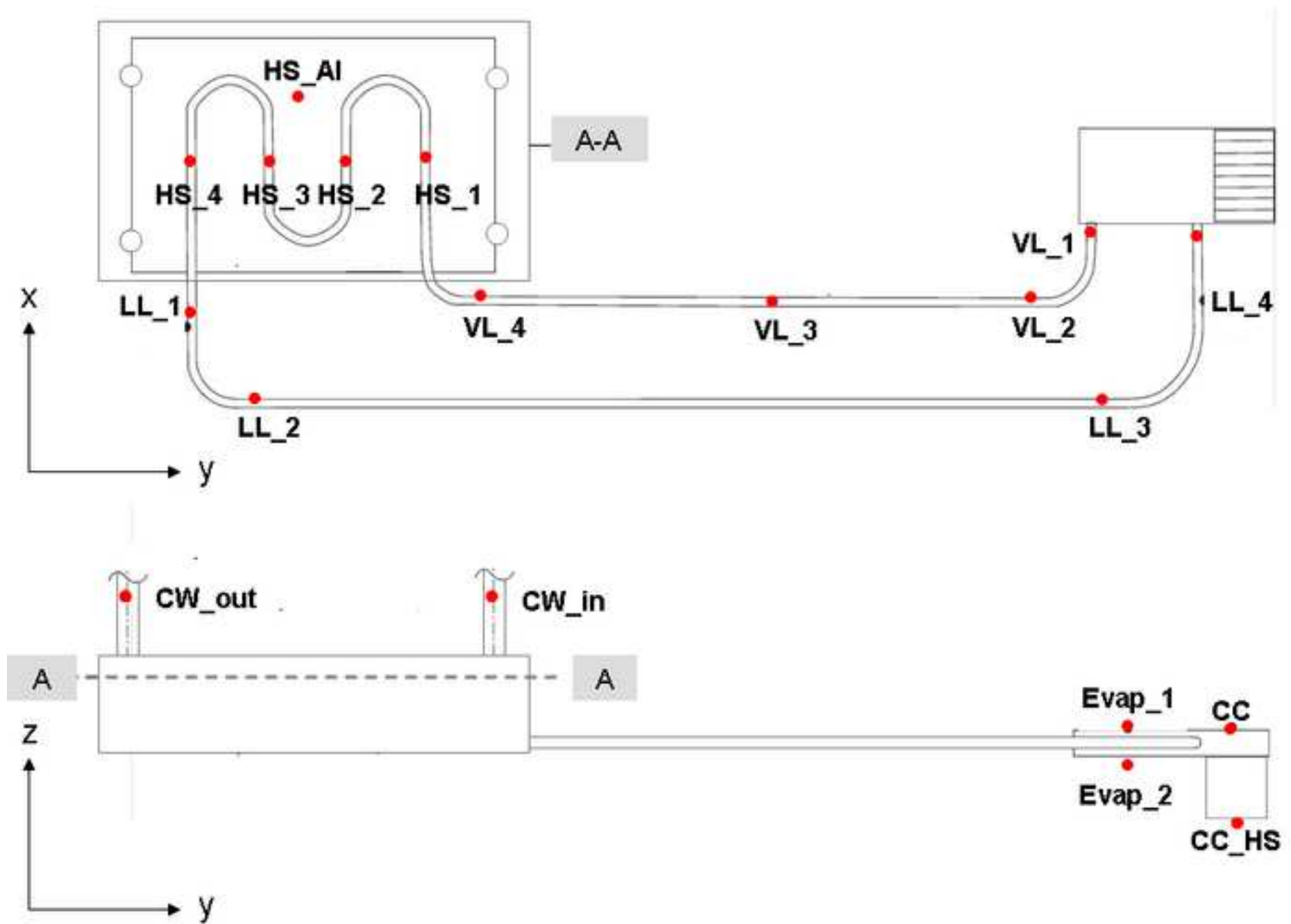
Figure(s)
[Click here to download high resolution image](#)



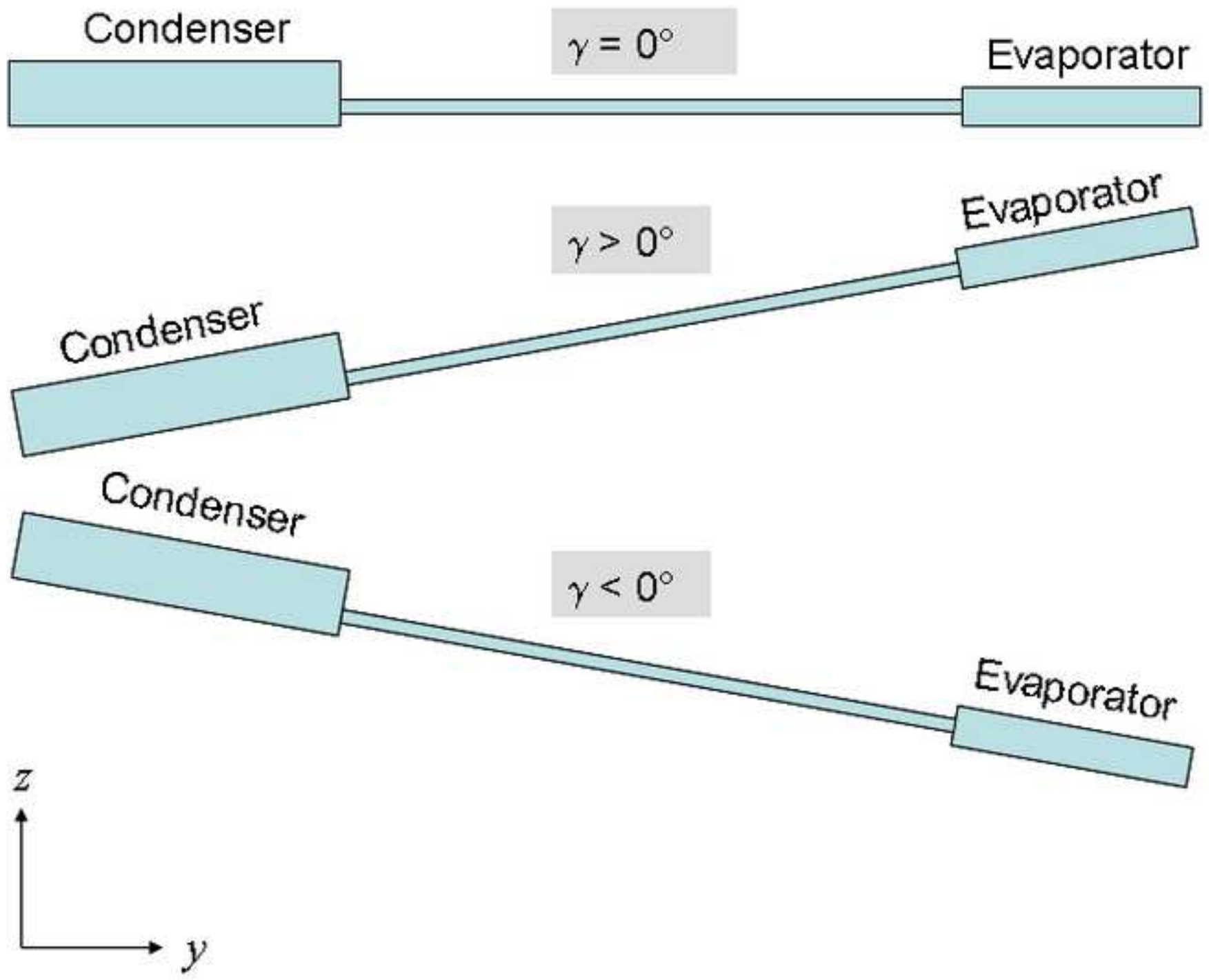
Figure(s)
[Click here to download high resolution image](#)



Figure(s)
[Click here to download high resolution image](#)

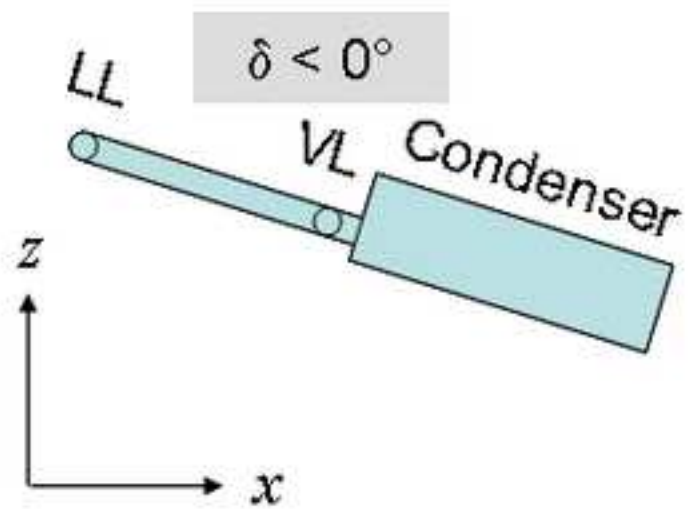
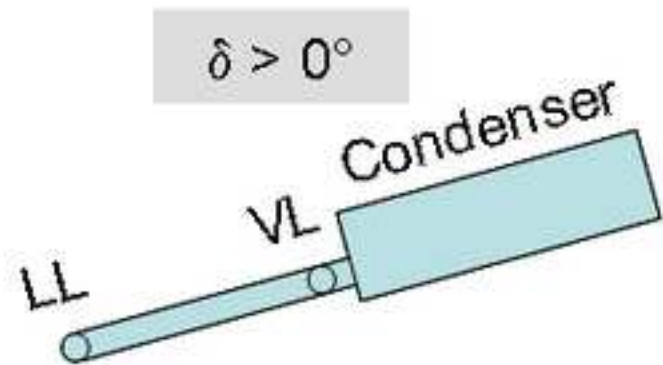
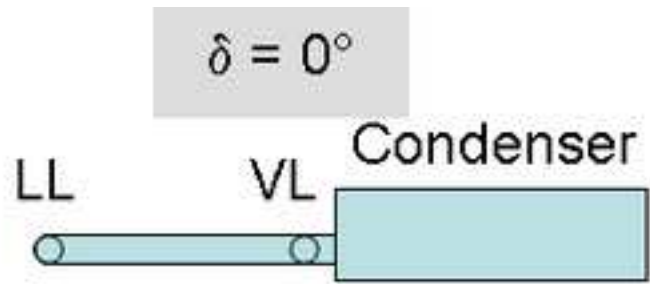


Figure(s)
[Click here to download high resolution image](#)

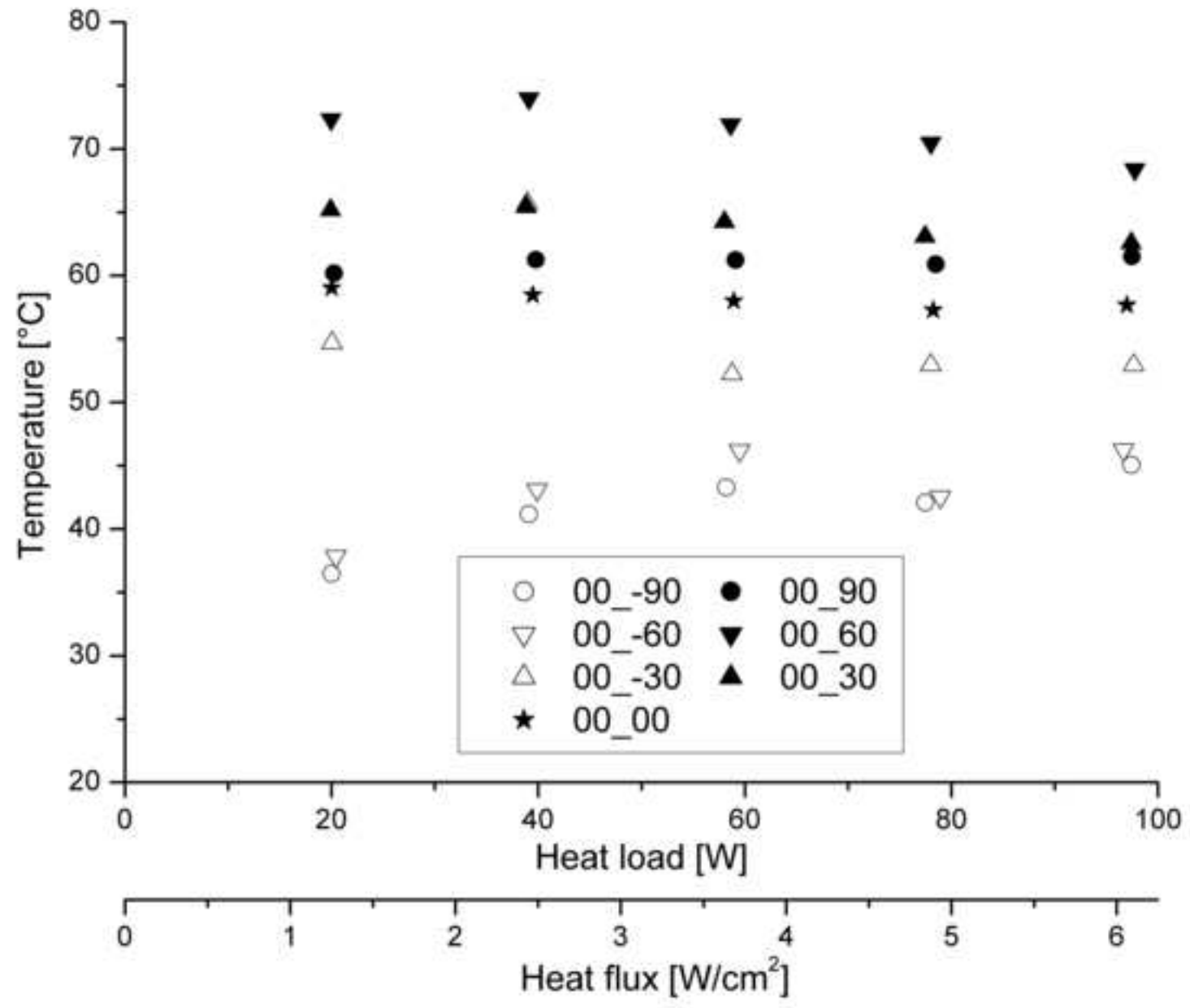


Figure(s)

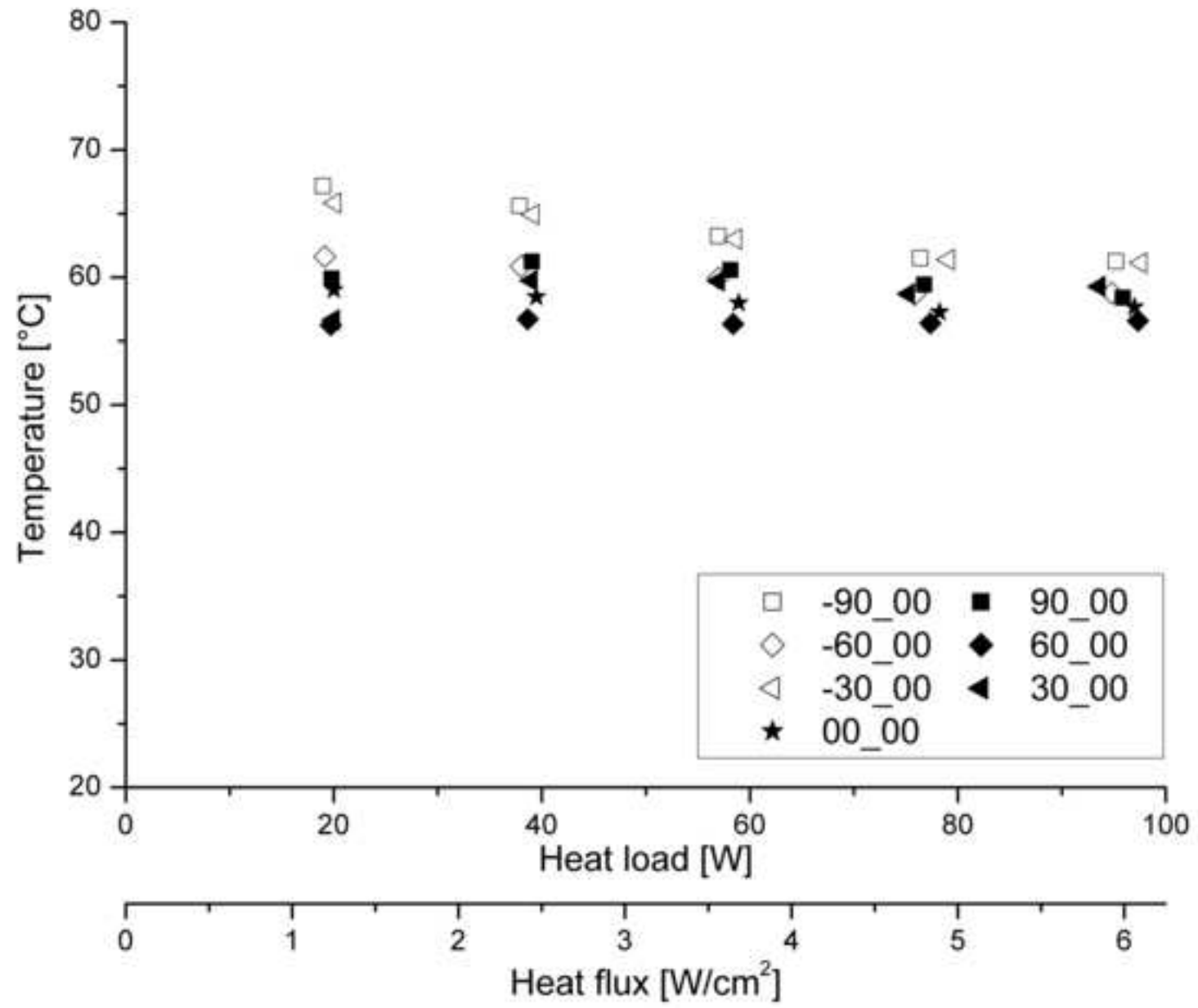
[Click here to download high resolution image](#)



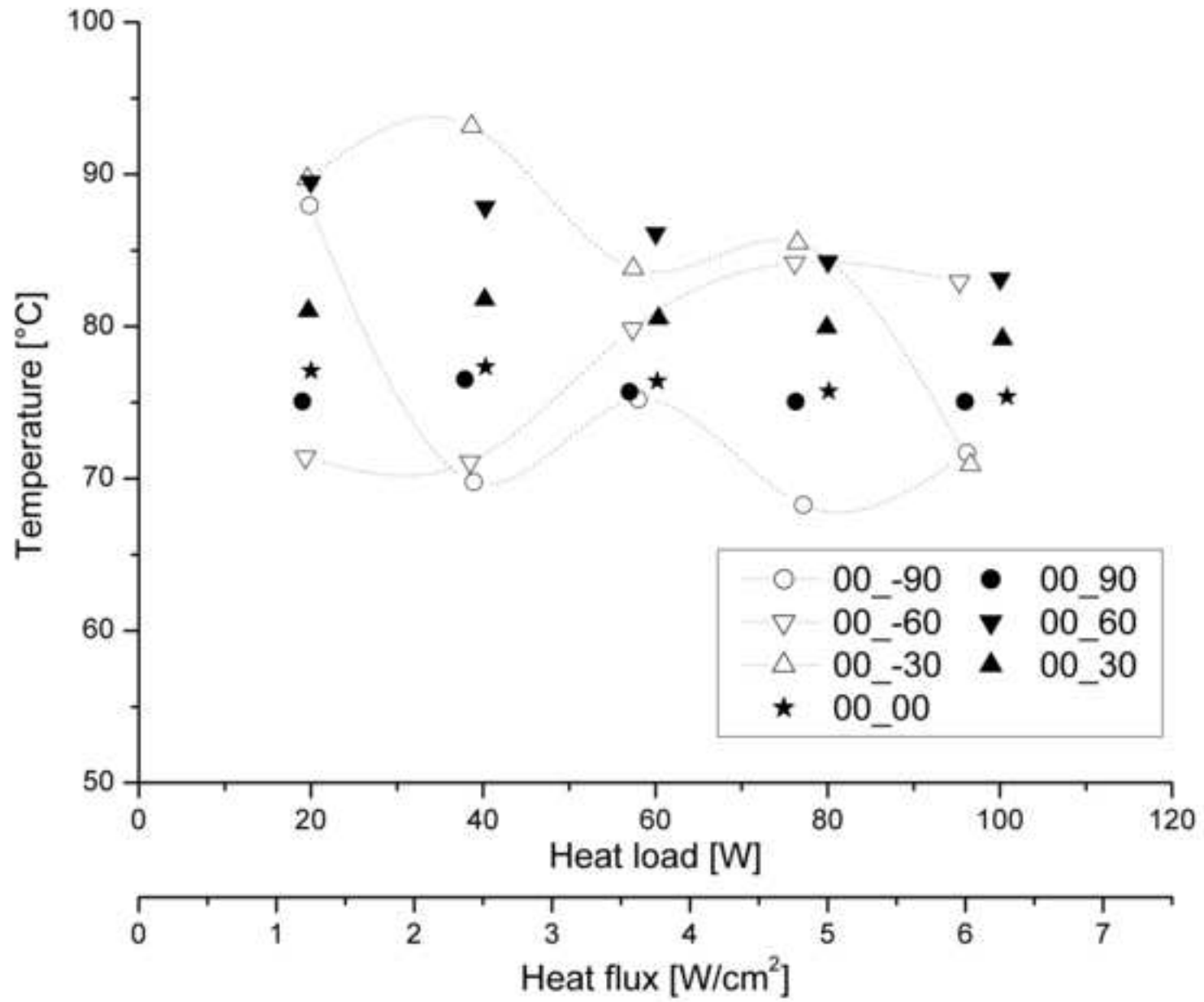
Figure(s)
[Click here to download high resolution image](#)



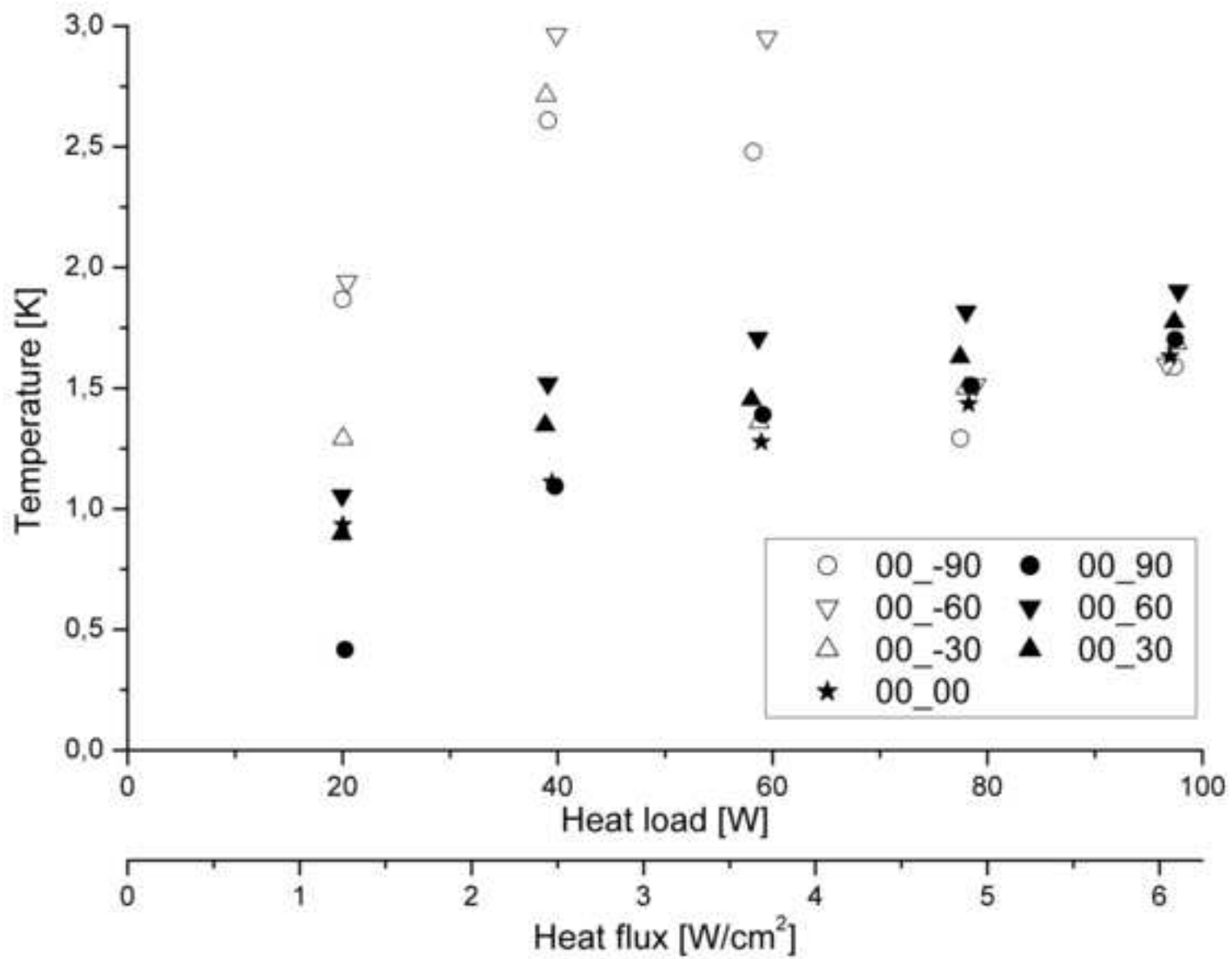
Figure(s)
[Click here to download high resolution image](#)



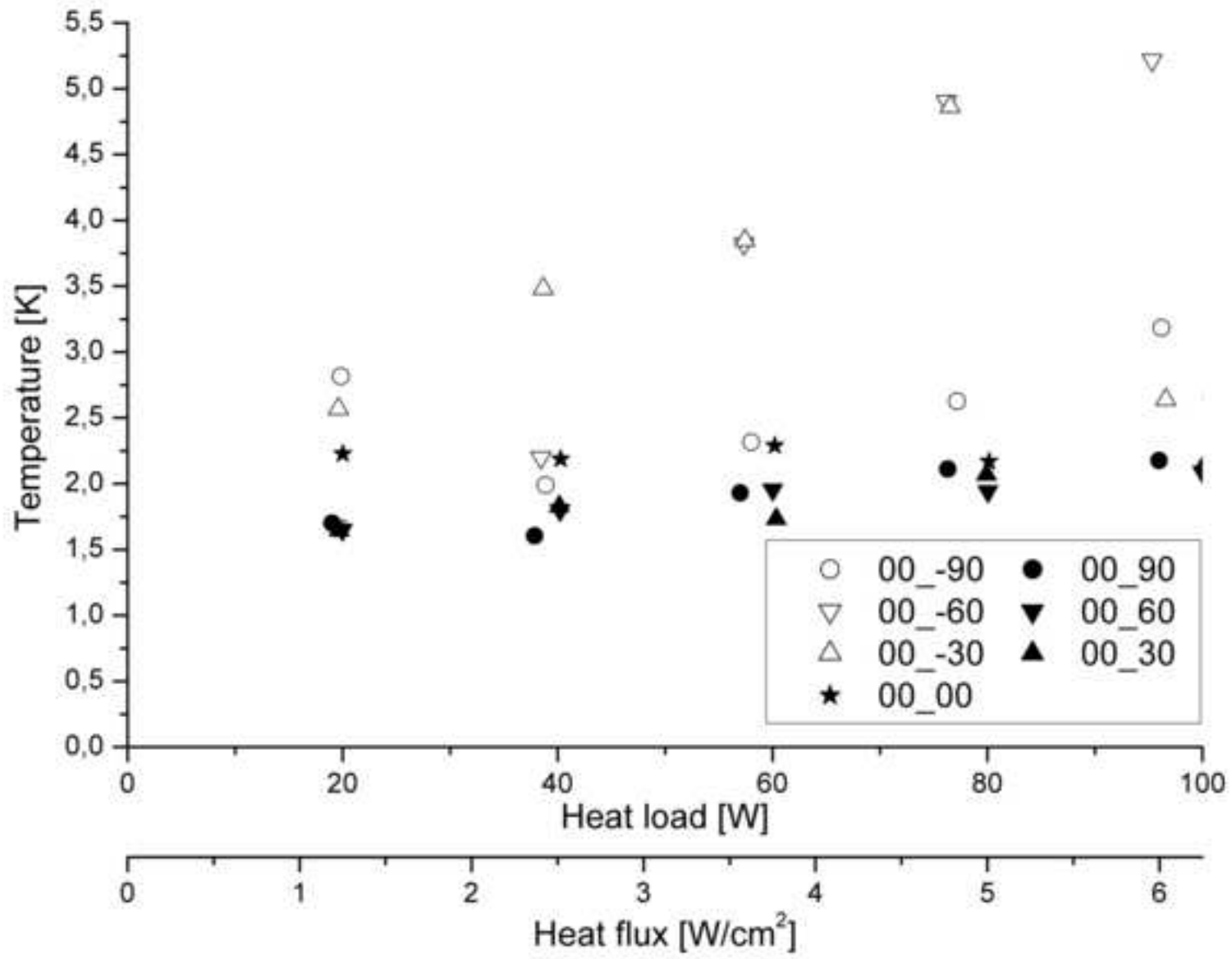
Figure(s)
[Click here to download high resolution image](#)



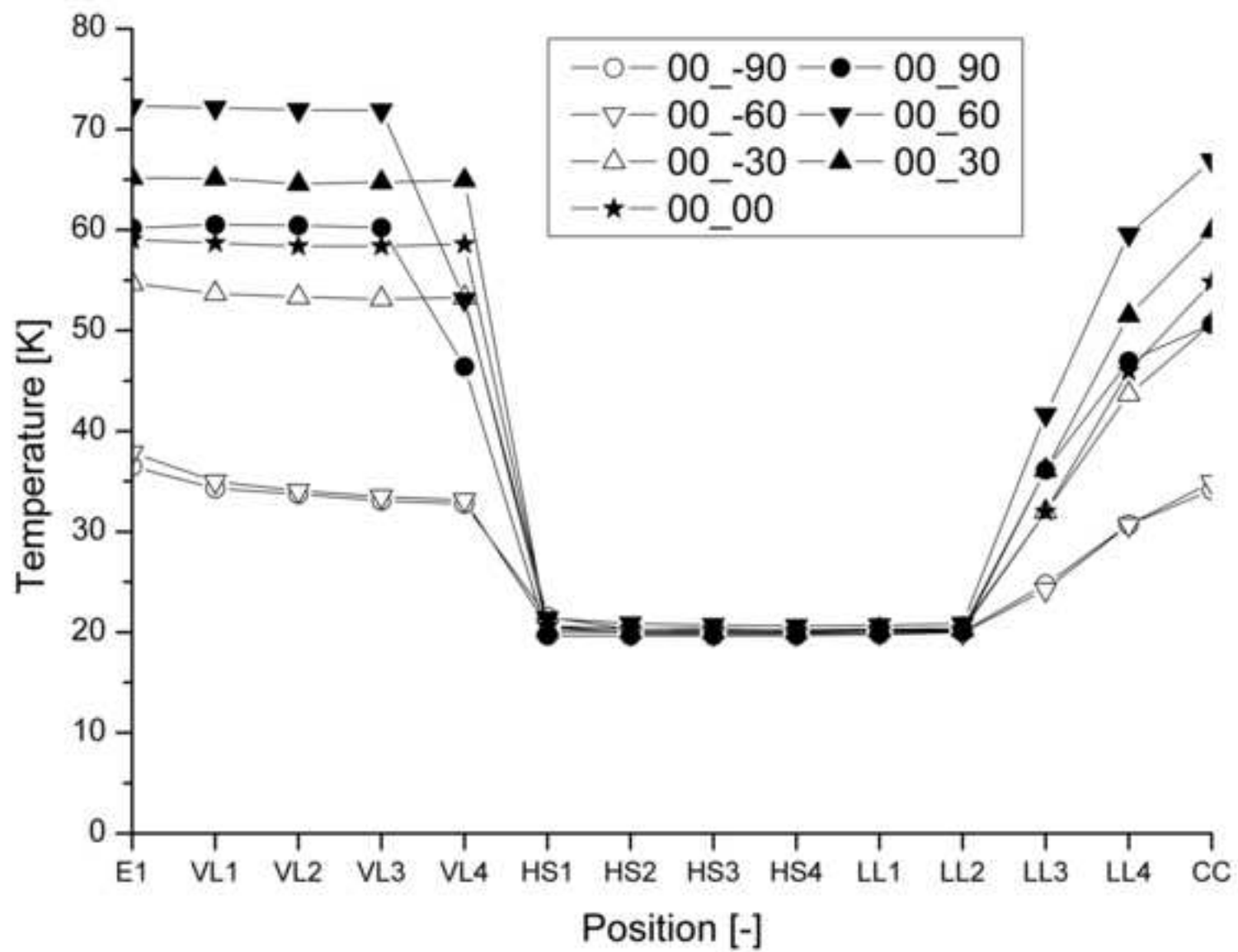
Figure(s)
[Click here to download high resolution image](#)



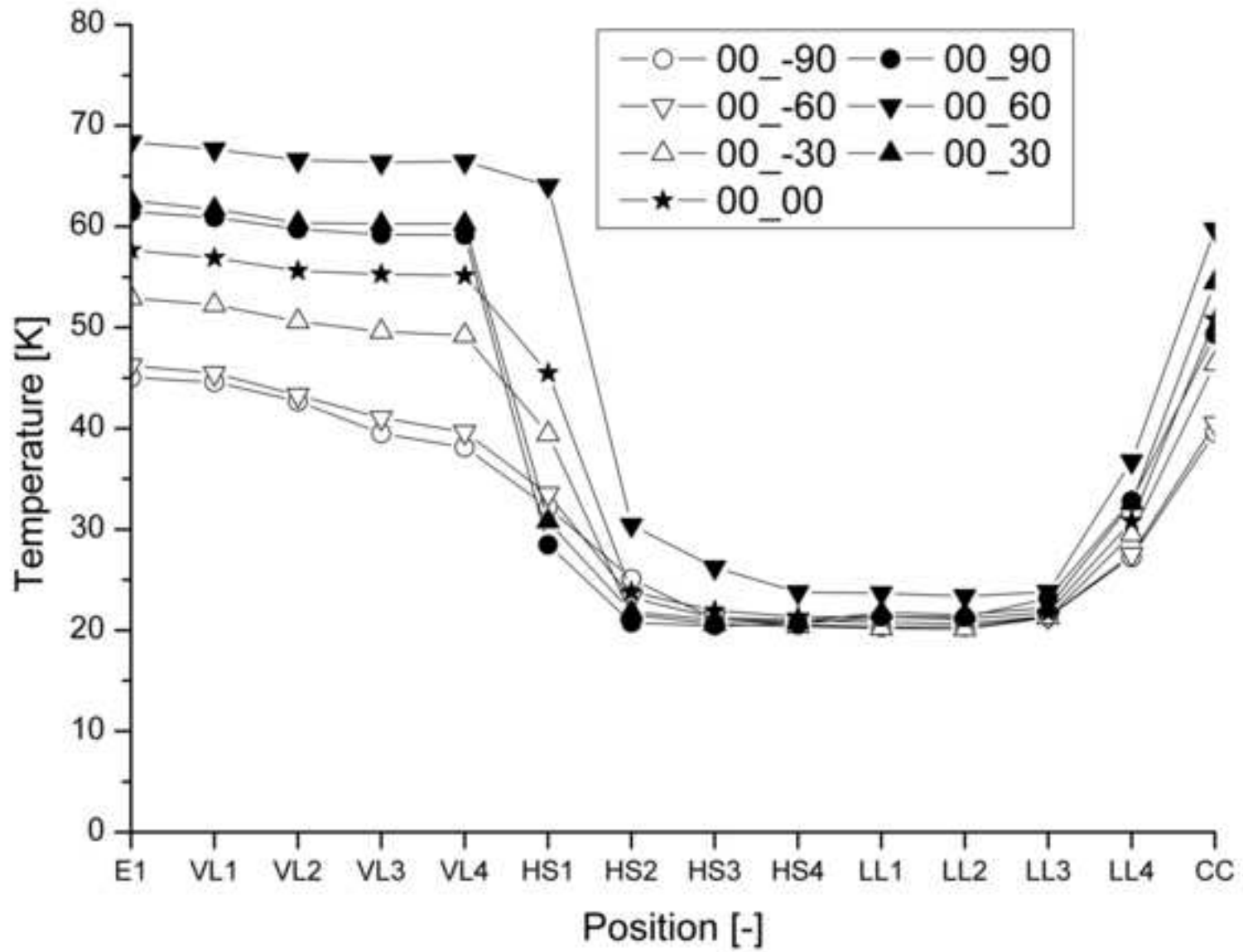
Figure(s)
[Click here to download high resolution image](#)



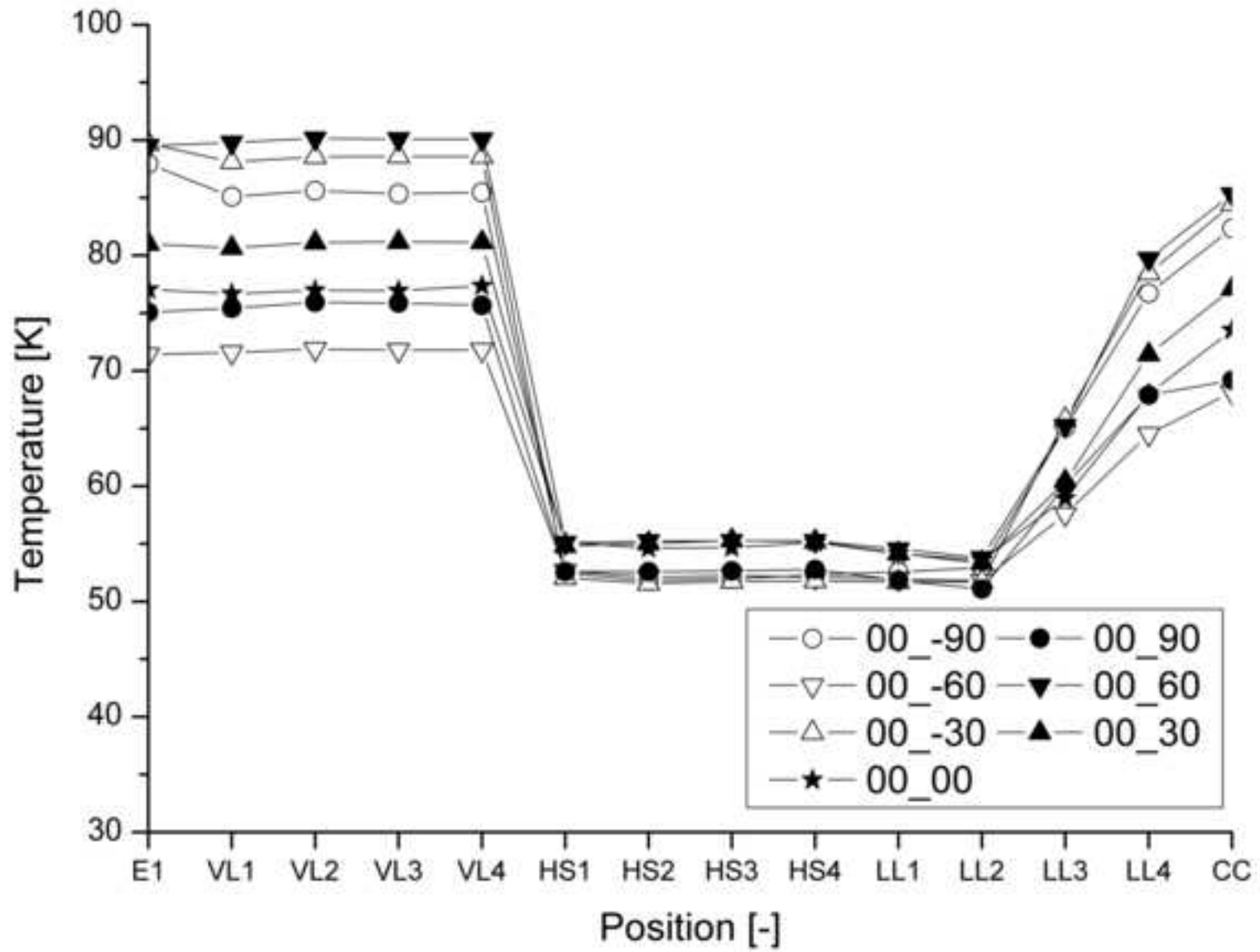
Figure(s)

[Click here to download high resolution image](#)

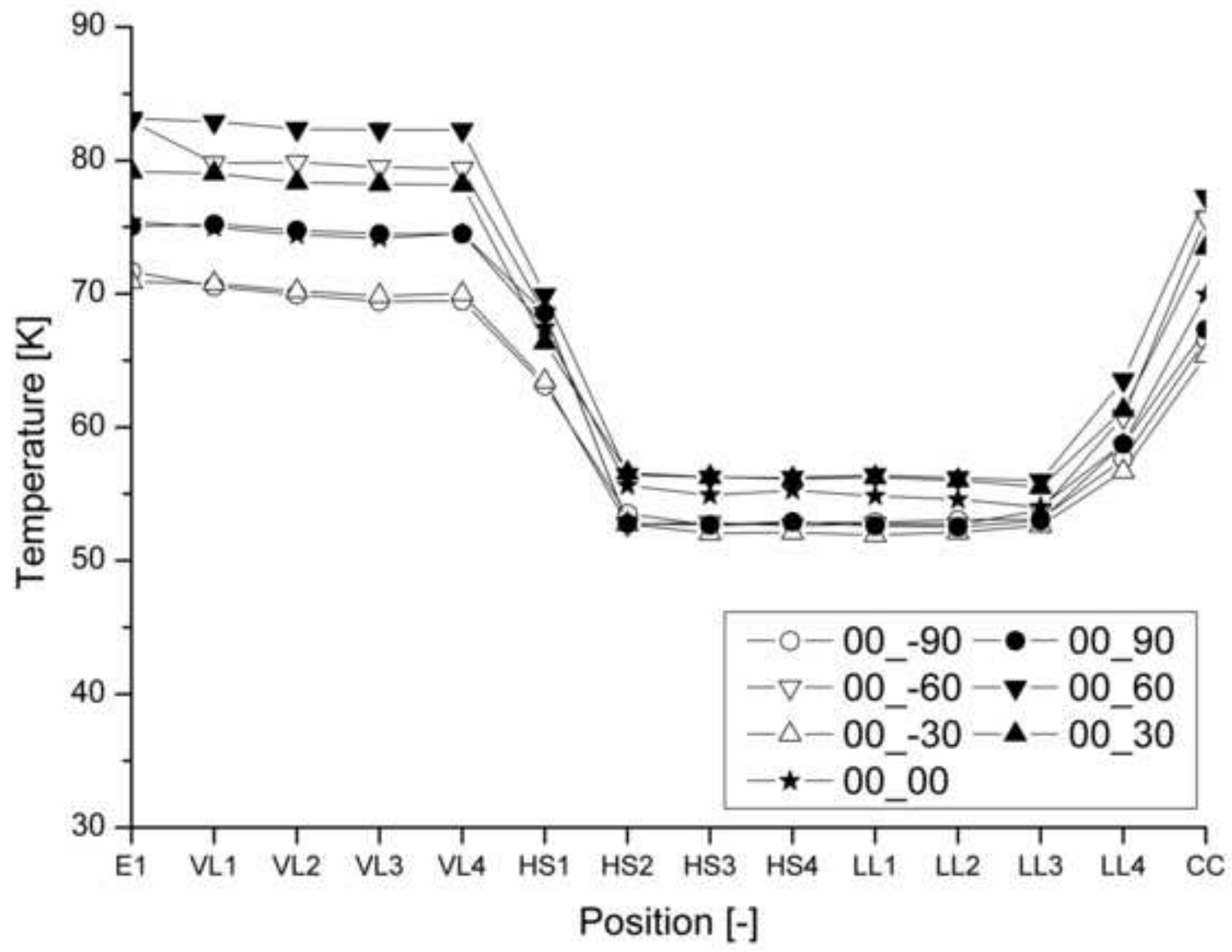
Figure(s)
[Click here to download high resolution image](#)



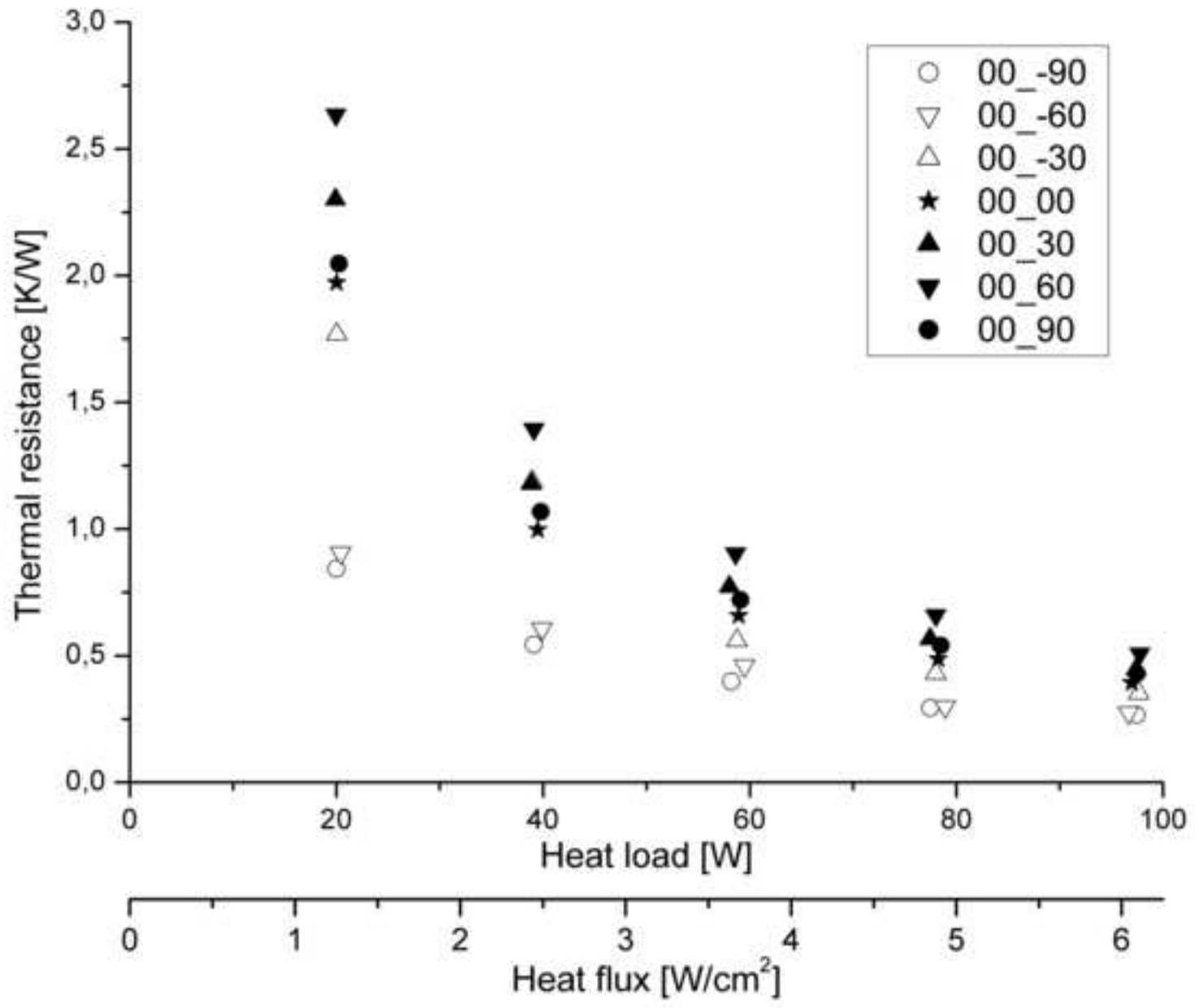
Figure(s)
[Click here to download high resolution image](#)



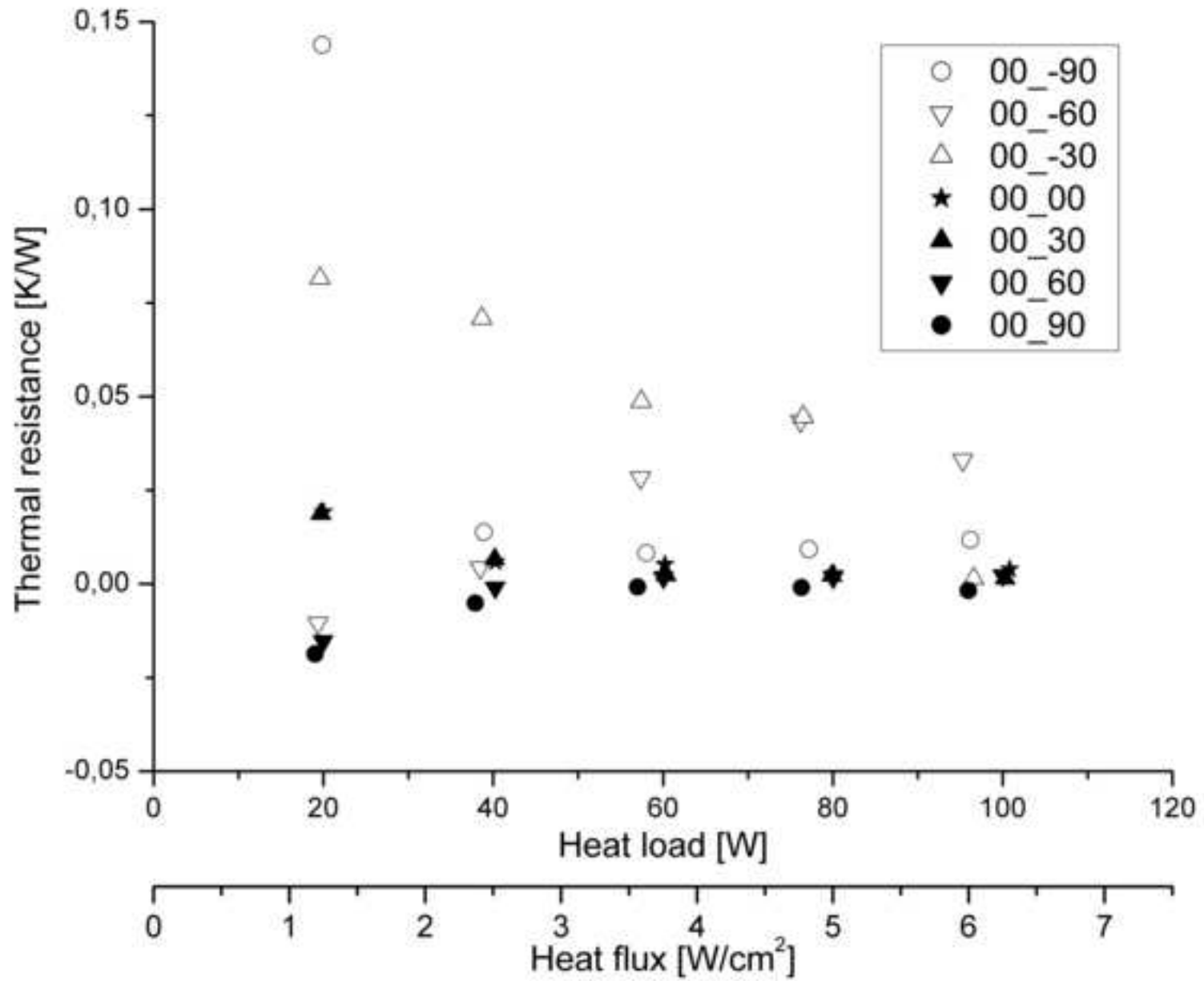
Figure(s)
[Click here to download high resolution image](#)



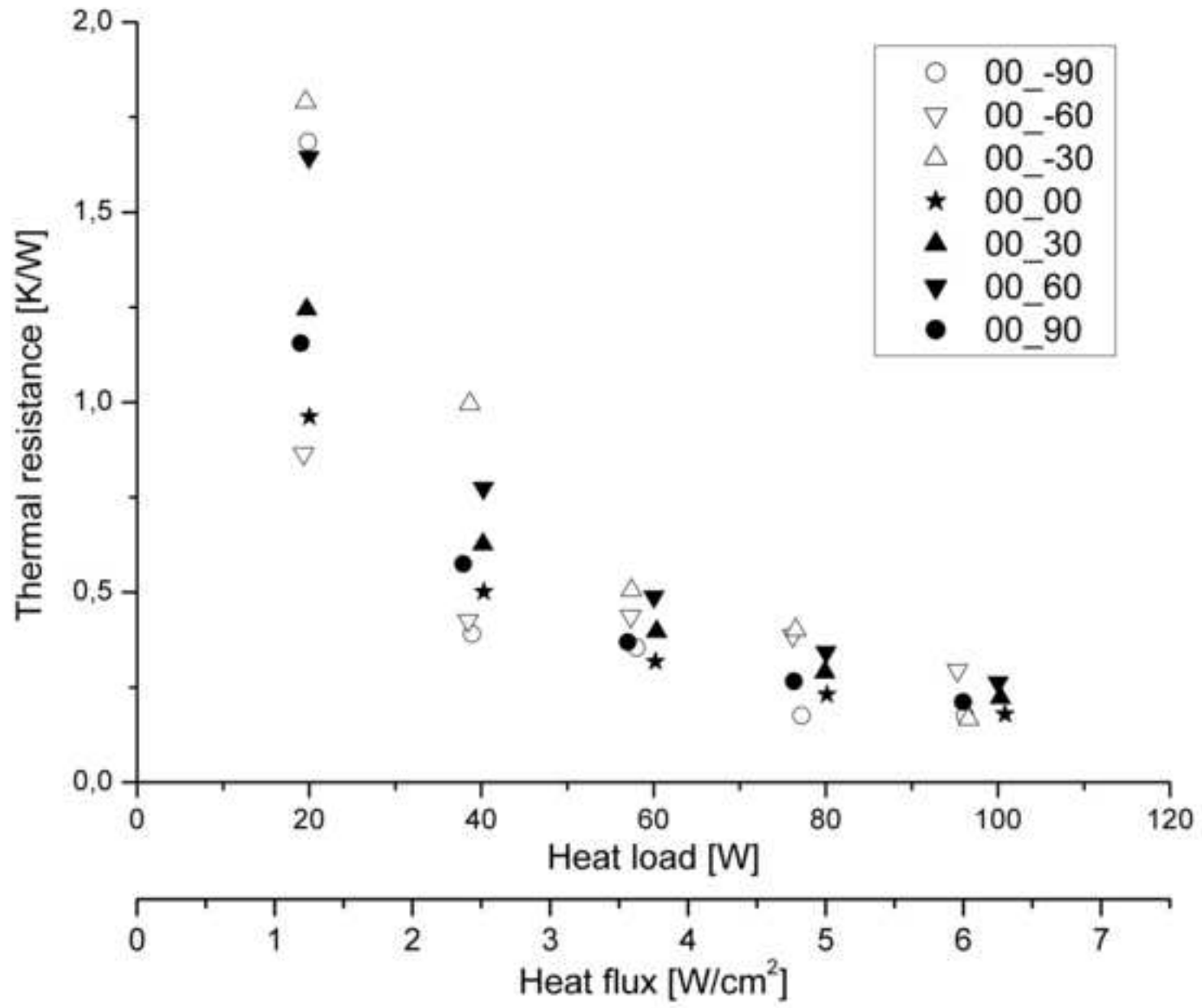
Figure(s)
[Click here to download high resolution image](#)



Figure(s)
[Click here to download high resolution image](#)



Figure(s)
[Click here to download high resolution image](#)



Evaporator	
Length [mm]	85
Width [mm]	42
Thickness [mm]	7
Body wall thickness [mm]	0.5
Wick	
Length [mm]	55
Porosity [%]	68.8
Pore breakdown radius [μm]	8.0
Compensation chamber	
Length [mm]	20
Vapour line	
Length [mm]	358
Diameter [mm]	4
Liquid line	
Length	765
Diameter	3
Condenser	
Length [mm]	562
Filling volume [cm^3]	19.24

Parameter	Variation / explanation
Type of cooling	Forced convection: <ul style="list-style-type: none"> · A condenser is attached to the condenser section with water as a coolant · Insulation along the loop heat pipe except at compensation chamber heat sink
Coolant temperature	$T_{Cool} = \{20;55\}^{\circ}C$
Box ambient temperature	$T_{Box,amb} = \{20;55\}^{\circ}C$
Orientation	Orientation in y-z direction γ <ul style="list-style-type: none"> · evaporator above condenser : positive angles · evaporator under condenser : negative angles · $\gamma = \{-90;-60;-30;0;+30;+60;+90\}^{\circ}$ Orientation in x-z direction δ <ul style="list-style-type: none"> · vapour line above liquid line: positive angle · vapour line under liquid line: negative angle · $\delta = \{-90;-60;-30;0;+30;+60;+90\}^{\circ}$
Power input	Electrical power input P_{el} $P_{el} = \{0;20;40;60;80;100\}W$